

## Article

# Introduction to Piezoelectric Actuators: Research Misconceptions and Rectifications - Part II

Kenji Uchino\*

*International Center for Actuators & Transducers, The Penn State University, University Park, PA 16802, USA*

*\*Correspondence: kenjiuchino@psu.edu*

### ABSTRACT

Piezoelectric actuator developments require interdisciplinary knowledge on materials physics, electrical designing and mechanical engineering. Because of the limited knowledge of newly-involved researchers, they occasionally publish misleading information, some sort of misconceptions, reflected in the delay of innovative developments of the next generation. This paper is Part II of a series of my tutorial course, and reviews the popular 10 among the researchers' misconceptions primarily related with the misunderstanding of 'voltage and electric field', 'ionic displacement and strain', 'thin film fabrication', 'energy transmission coefficient', 'thin film device designing', 'piezoelectric vibration damping', 'mechanical impedance matching', 'piezoelectric energy harvesting', 'resonance & anti-resonance', 'best-selling devices', and provides rectifications, aiming at their future progress.

**KEYWORDS:** Piezoelectric actuator; Strain; Efficiency; Energy transmission coefficient; Mechanical impedance matching; Resonance/antiresonance; Piezoelectric energy harvesting

**Received:** Oct. 7<sup>th</sup>, 2019

**Accepted:** Dec. 19<sup>th</sup>, 2019

**Online:** Jan. 8<sup>th</sup>, 2020

## 1. Introduction

Uchino authored an instructor's manual "Ferroelectric Devices & Piezoelectric Actuators<sup>[1]</sup>" (DEStech Pub. Inc., 2017) for helping with instructors' teaching "Ferroelectric Devices" and "Micromechanics" courses, using the textbooks<sup>[2,3]</sup> titled exactly the same name published from CRC Press in 2010 and 2019, respectively. I wrote one chapter on "Research Misconceptions and Rectifications" for the sake of improving their instruction skills. However, thanks to many professors' request, I decided to publish it as a journal paper for wider readers, "Introduction to Piezoelectric Actuators: Research Misconceptions and Rectifications", Japan. J. Appl. Phys. this year<sup>[4]</sup>. I have been receiving many acknowledgements from worldwide researchers. Because they are already professors or senior researchers, they might have hesitated to ask the fundamental questions to other colleagues. Knowing this situation, Uchino decided to author Part II of "Research Misconceptions and Rectifications" in this journal "Insight – Material Science" as the Editor-In-Chief. Since the misconceptions come from almost the same fundamental points in "piezoelectricity", the rectifications are similar to the previous articles inevitably. However, in this article Uchino focused on the misconceptions collected recently from the actual journal papers already published after peer-review; that means, both authors and reviewers have a similar problem. Pardon me if the "Questions" below are cited from your publication. Uchino is not intending to accuse these authors, but cited them merely due to common misconceptions of present researchers in our piezoelectric fields.

## 2. Researcher’s common misconceptions

Piezoelectric actuator developments require interdisciplinary knowledge on materials physics, electrical designing and mechanical engineering, and now thin film MEMS (micro electro-mechanical system) researchers, are primarily approaching. Because of limited knowledge of newly-involved professors, they occasionally instruct the students with a sort of misconception, reflecting to the delay of innovative developments in the next generation. This paper reviews the popular 10 among these common misconceptions found in published articles, which are primarily related with the misunderstanding of ‘voltage and electric field’, ‘ionic displacement and strain’, ‘thin film fabrication’, ‘energy transmission coefficient’, ‘thin film device designing’, ‘piezoelectric vibration damping’, ‘mechanical impedance matching’, ‘piezoelectric energy harvesting’, ‘resonance & anti-resonance’, ‘best-selling devices’.

If you do not find suitable answers in the following questions, you are a sort of patient, and you had better read through this tutorial article further, in addition to Part I in the previous articles, as a prescription for your successful future development. As the author’s experience, 44 years as a university professor, 21 years as a company president or VP, 7 years as a government program officer, I have a solid philosophy: “Without a strong fundamental understanding, no break-through invention comes out”.

### 2.1 Voltage and electric field

**Question 1:** The polarization  $P$  versus electric field  $E$  relation in a PZT specimen shown in **Figure 1(a)** (solid line) is cited from a journal paper written by a famous professor. He argued that “the internal positive electric field bias was observed in the  $P$ -  $E$  hysteresis”. Consider what is wrong about his claim, and why this mistake happens.

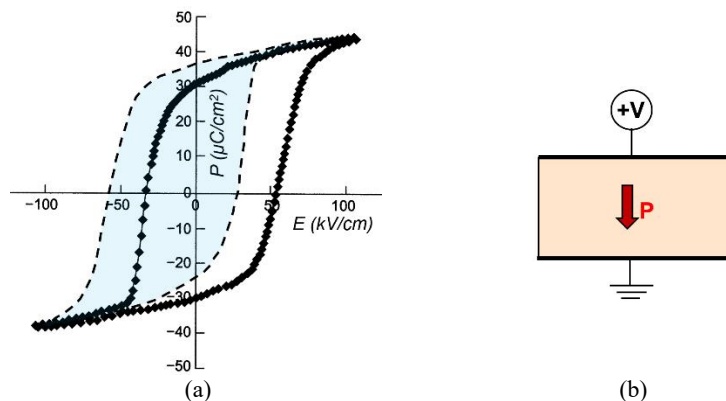


**Figure 1.** (a) Biased  $P$ - $E$  hysteresis curves: Original figure on the paper (solid line), and corrected figure (dashed line). (b) Voltage and poling direction.

**Solution:** Researcher’s common misconception include the confusion among voltage and electric field. Though this is learned in the high school age, practical training seems to be missing. Supposing a PZT disk with top and bottom surfaces electroded, when we apply high DC voltage on the top by keeping the bottom electrode ground (see **Figure 1(b)**), is this disk poled upward or downward? The correct answer is ‘downward’. You learned the relationship between electric field and voltage:  $E = -\text{grad}(V)$ . If we believe this solid-line  $P - E$  hysteresis curve measurement correct, we need to conclude that the ‘negative electric field bias’ is observed in the hysteresis curve, because this specimen needs just a small negative field to realize the polarization reversal to  $-P_S$ , while a much larger positive field to realize the another polarization reversal to  $+P_S$ . However, this paper’s content needs the conclusion of ‘positive field bias’. So, what is wrong with his measured  $P - E$  curve? During a practical measurement using a Sawyer-Tower circuit, a researcher usually obtains the voltage  $V$  vs. charge  $Q$  relation, and most of the researcher will take positive voltage in the rightward direction. The problem usually exists in the next step; that is, during changing voltage to electric field.

Many researchers usually change the horizontal scale by dividing the voltage  $V$  by the specimen thickness  $t$ , without changing the hysteresis curve shape. If you remember that field is given by  $E = -\text{grad}(V)$ , you can easily understand that electric field is obtained by  $(-V/t)$ , or you need to plot  $E$  in the opposite direction to the voltage axis. In practice, the hysteresis curve should be rotated by 180 degree with respect to the origin (0,0), which is shown by the dashed line on **Figure 1(a)**, where you can find now the ‘positive’ bias field correctly. Probably his research assistant made this primitive mistake on the axis direction exchange during  $V \rightarrow -E$ .

**Reminder:** Do not forget “minus” when you convert;  $E = -V/t$ .

## 2.2 Ionic displacement and strain

**Question 2:** A famous encyclopedia’s description: “Electrostriction is caused by a slight displacement of ions in the crystal lattice under a field. This displacement will accumulate throughout the bulk and result in an overall strain along the field.” Is this true or false? Explain what is the misconception on this description.

**Solution:** Why a strain is induced by an electric field is explained herewith. For simplicity, let us consider the simplest ionic crystal such as NaCl<sup>[2]</sup>. **Figure 2** shows a rigid-ion spring 1-D model of the crystal lattice, where the springs connecting cations and anions represent equivalently the cohesive force resulting from the electrostatic Coulomb energy and the quantum mechanical repulsive energy. **Figure 2(a)** shows a non-centrosymmetric general case, whereas **2(b)** shows a centrosymmetric case. In (a), the springs joining the ions can be different for the shorter and longer ionic distances; in other words, hard and soft springs may exist alternately; whereas in (b), the springs joining the ions should be all the same because of the crystal symmetry.

We consider first the state of the crystal lattice shown in **Figure 2(a)** where two ‘hard’ and ‘soft’ springs can be aligned alternatively. When we apply an applied electric field externally on this crystal (right-ward on the figure), the cations are drawn in the direction of the electric field and the anions in the opposite direction, leading to the relative change in the inter-ionic distance. Depending on the direction of the electric field, the soft spring expands or contracts more than the contraction or expansion of the hard spring, respectively, causing a strain  $x$  (a unit cell length change) in proportion to the electric field  $E$ . This is the converse piezoelectric effect. When expressed as

$$x = d E, \tag{1}$$

the proportionality constant  $d$  is called the piezoelectric constant.

On the other hand, in **Figure 2(b)**, the amounts of extension and contraction of the spring are nearly the same (though ionic displacements are similar to **Figure 2(a)**!), and the distance between the two cations (lattice parameter) remains almost the same, hence, there is zero strain! However, more precisely, ions are not connected by such idealized springs (those are called harmonic springs, in which force ( $F$ ) = spring constant ( $k$ )  $\times$  displacement ( $\delta$ ) holds). In most cases, the crystal springs possess anharmonicity ( $F = k_1\delta - k_2\delta^2$ ); that is, they are somewhat easy to extend, but hard to contract (because of significantly large quantum mechanical potential during squeezing). Such subtle differences in the displacement causes a change in the lattice parameter, producing a strain which is independent of the direction of the applied electric field ( $+E$  or  $-E$ ), and hence is an even-function of the electric field. This is called the electrostrictive effect, and can be expressed as

$$x = M E^2, \tag{2}$$

where  $M$  is the electrostrictive constant. Note that a small electrostriction crystal does not mean small ionic displacement, but that the anharmonicity of the crystal springs is small.

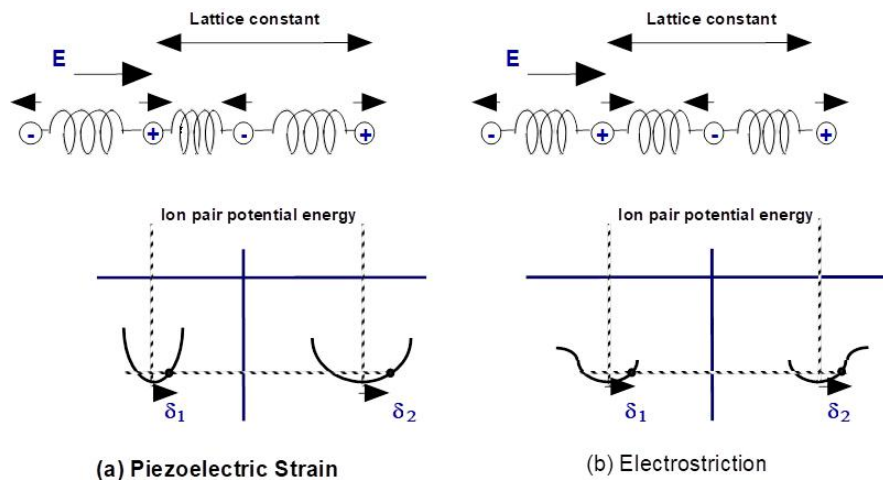


**Figure 2.** Microscopic explanation of the piezoelectric and electrostriction.

**Reminder:** Though the ionic displacements ( $\delta$ ) in (a) and (b) are similar, the strain (*differentiation of the displacement* ( $\partial\delta/\partial x$ )) is very different. Strain is NOT the accumulation of ion displacement, but the subtraction or differentiation!

### 2.3 Thin film fabrication

**Question 3:** The following sentences can be occasionally found in the MEMS (micro electro-mechanical system) papers: “When we fabricate PZT thin films, the substrate, the lattice parameter of which is close to that of the PZT, should be chosen without creating the lattice parameter mismatch on the interface, in order not to degrade the piezoelectric film performances.” The reason why they are following this approach is commonly provided because “the previous researchers did so.” Is this really a good strategy to follow? Is there any possibility to enhance the performance by taking the “large” lattice parameter mismatch?

**Solution:** The thin film structure is inevitably affected by four important factors:

- (1) Size constraints: Similar to a powder sample, there may exist a critical film thickness below which the ferroelectricity would be degraded significantly or might disappear, though the thin films are energy-stabilized with large 2D area.
- (2) Stress from the substrate: The lattice parameter mismatch between the substrate and PZT generates dislocations on the PZT thin film, leading to degradation of the film performance, and tensile or compressive stress is generated due to thermal expansion mismatch between the film and the substrate, leading to sometimes a higher coercive field for domain reorientation.
- (3) Epitaxial growth: Crystal orientation dependence should also be considered, similar to the case in single crystals. An example can be found in a rhombohedral composition PZT, which is supposed to exhibit the maximum performance when the  $P_s$  direction is arranged  $57^\circ$  cant from the film normal direction (*i.e.*, (001) perovskite crystallographic orientation). Refer to the previous paper<sup>[5]</sup>.
- (4) Preparation Constraint: Si substrate requires low sintering temperature of the PZT film. Typically  $800^\circ\text{C}$  for a short period is the maximum for preparing the PZT, which may limit the crystallization of the film, leading to the reduction of the properties.

Wasa investigated piezoelectric performance enhancement by using the crystal lattice mismatch intentionally of PZT-based thin films on Si and sapphire<sup>[6]</sup>. Referring to **Figure 3(a)**, the lattice mismatch statuses between the thin film and substrate are considered in the case that the lattice parameter of the piezoelectric film is larger than that of the substrate. When we deposit the film on the substrate, the film will impose compressive stress in the plane direction. However, if the *misfit rate* is large, dislocations may be generated in every certain-unit lattices. Since the dislocation degrades the

piezoelectric performance significantly, most of researchers used to try to reduce the mismatch rate between the film and substrate. Wasa's group proposed an innovative preparation method of the strained thin film on the substrate without dislocation. **Figure 3(b)** illustrates their idea with using 1.7° angled surface of the substrate to deposit PZT film. Because the PZT interface plane changes one-step height every 30 horizontal unit-cells. The lattice misfit stress can be relaxed without generating significant dislocations. This angle can be different, depending on the lattice misfit rate. They demonstrated the PZT films under high compressive stress without dislocation with the Curie temperature as high as 600°C, 250°C higher than its original Curie temperature under zero stress. The reader may know that Curie temperature can be shifted with a rate 50°C per 1 GPa under hydrostatic pressure, which may be utilized intentionally to improve the film performance.

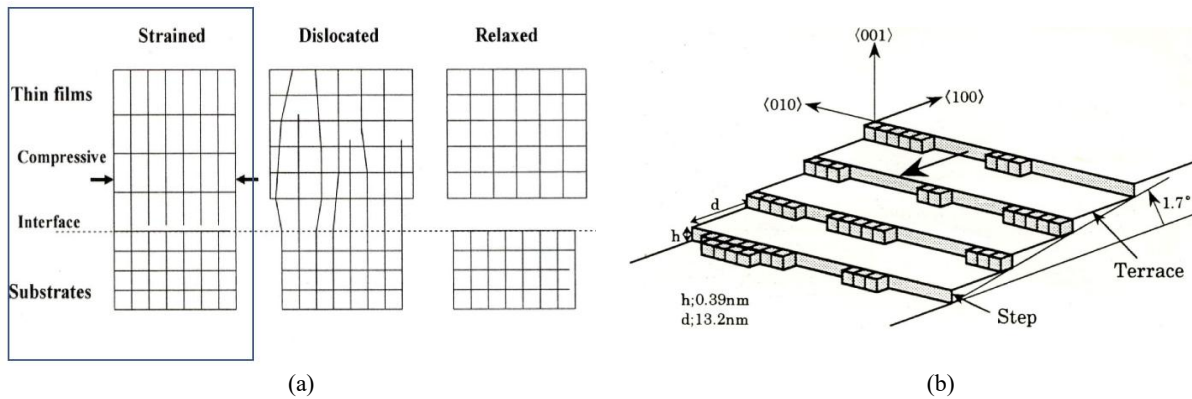


**Figure 3.** (a) Lattice mismatch statuses between the thin film and substrate. (b) Preparation method of the strained thin film on the substrate without dislocation<sup>[6]</sup>.

**Reminder:** When you fabricate PZT films, consider to utilize the tensile or compressive stress intentionally, but without generating dislocations by using a slight cant angle of the substrate<sup>[6]</sup>.

## 2.4 Energy transmission coefficient

**Question 4:** A paper authored by a mechanical engineering professor described: “A ‘*coupling coefficient*’ is a measure of the ‘*efficiency*’ with which a piezoelectric material converts the energy in an imposed signal to useful mechanical energy,” and “By applying 1 J of electric energy to a piezoelectric with an electromechanical coupling factor  $k$ , we accumulate  $k^2$  J of mechanical energy in this piezo-material. Thus, this actuator can work mechanically up to  $k^2$  J to the outside, and the efficiency is considered to be  $k^2\%$ .” These sentences include two major misconceptions. Describe them and provide their rectifications.

**Solution:** This is typical misconceptions by a mechanical engineering researcher, because they may not know how to recover the electrostatic energy from a piezoelectric. Three confusing terminologies are introduced in this subsection.

### 2.4.1 Electromechanical coupling factor

First of all, remember the following constitutive equations:

$$D = \epsilon^X E + dX \quad (3)$$

$$x = dE + s^E X \quad (4)$$

where  $d$  is the piezoelectric constant,  $s^E$ , elastic compliance under short-circuit condition, and  $\epsilon^X$  is the permittivity under stress-free condition. Then, the electromechanical coupling factor  $k$  is defined by

$$k^2 = d^2 / s^E \epsilon^X. \quad (5)$$

The value  $k^2$  has a meaning of *energy conversion rate*, that is,

$$k^2 = (\text{Stored mechanical energy}) / (\text{Input electrical energy}). \quad (6a)$$

or

$$k^2 = (\text{Stored electrical energy})/(\text{Input mechanical energy}). \quad (6b)$$

Taking an example value  $k = 50\%$  for a piezoelectric pseudo-DC device,  $k^2 = 25\%$ , then the input electrical energy 100 is converted into mechanical energy 25, by remaining  $(1 - k^2) 74$  as stored electrical energy (in a capacitor). Because the loss factor (dielectric loss  $\tan \delta$ ) is less than 1%, actual loss dissipated as heat is usually less than 1%. The energy conversion process is visualized in **Figure 4(a)**. Thus, if we can collect the stored electrical energy back to the drive circuit, we can declare that the loss is only 1%.

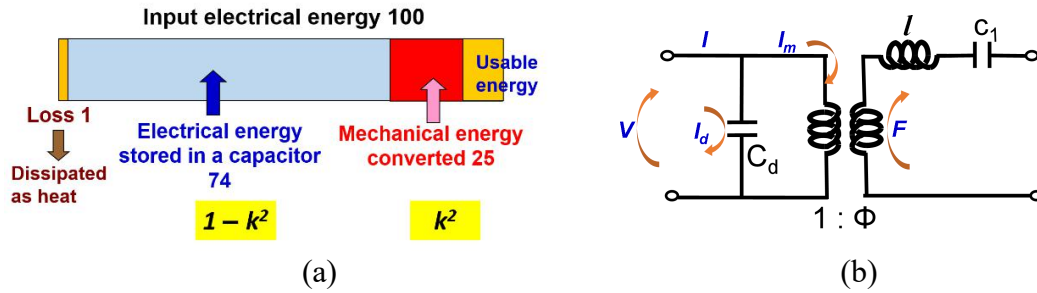


**Figure 4.** (a) Energy conversion rate in a typical piezoelectric. (b) Equivalent circuit ( $k_{31}$  mode).

## 2.4.2 Energy transmission coefficient

Not all the mechanically stored energy can actually be used, and the actual work done depends on the mechanical load (**Figure 4(a)**). With zero mechanical load or complete clamp condition (*i.e.*, no strain), no output work is done or no energy is spent to the outside. The *energy transmission coefficient* is defined by

$$\lambda_{max} = (\text{Output mechanical energy}/\text{Input electrical energy})_{max} \quad (7a)$$

or equivalently,

$$\lambda_{max} = (\text{Output electrical energy}/\text{Input mechanical energy})_{max} \quad (7b)$$

The difference of the above from **Eqs. (6)** and **(7)** is “stored” or “output/spent”.

Let us consider the simplest case where an electric field  $E$  is applied suddenly to a piezoelectric under constant external stress  $X$  ( $<0$ , compressive stress). This corresponds to the situation that force and voltage are applied on the actuator with a ‘step’ function, not a gradual application, as shown in **Figure 5(a)**<sup>[2]</sup>. **Figure 5(b)** shows two electric-field versus induced-strain curves, corresponding to two conditions; under the mass load and no mass. Because the area on the field-strain domain does not mean the energy, we should use the stress-strain and field-polarization domains separately in order to discuss the mechanical and electrical energy, respectively. The mechanical energy calculation process is illustrated in **Figure 5(c)**. Note that the mass shrinks the actuator first by  $sX$  ( $s$ : piezo-material’s compliance, and  $X < 0$ ). This mechanical energy  $sX^2$  is a sort of “loan” of the actuator credited from the mass, which should be paid back or subtracted later. This energy corresponds to the hatched area in **Figure 5(c)**. By applying the step electric field, the actuator expands by the strain level  $dE$  under a constant stress condition. This is the mechanical energy provided from the actuator (electromechanically transduced energy) to the mass, which corresponds to  $|dEX|$ . Like paying back the initial “loan”, the output work (from the actuator to the mass) can be calculated as the area subtraction (shown by the dotted area in **Figure 5(c)**)

$$\int (-X) dx = -(dE + sX) X. \quad (8)$$

On the contrary, **Figure 5(d)** illustrates the electrical energy calculation process. The mass load  $X$  generates the “loan” electrical energy by inducing  $P = dX$  (see the hatched area in **Figure 5(d)**). By applying a ‘step’ function electric field  $E$ , the actuator (like a capacitor) receives the electrical energy of  $\epsilon_0 \epsilon E^2$ . Thus, the total energy is given by the area subtraction (shown by the dotted area in **Figure 5(d)**)

$$\int (E) dP = (\epsilon_0 \epsilon E + dX) E. \quad (9)$$

Now, we need to choose a proper load to maximize the *energy transmission coefficient*, defined by the ratio between **Eqs. (8)** and **(9)**. From the maximization condition of



$$\lambda = - (d E + s X) X / (\epsilon_0 \epsilon E + d X) E,$$

we can obtain

$$\lambda_{max} = [(1/k) - \sqrt{(1/k^2) - 1}]^2 = [(1/k) + \sqrt{(1/k^2) - 1}]^{-2}. \quad (10)$$

The detailed derivation process is given in Ref [3]. We can obtain from Eq. (10) for a reasonable  $k$  (< 95%) that

$$k^2/4 < \lambda_{max} < k^2/2.$$

For a small  $k$ ,  $\lambda_{max} = k^2/4$ , and for a large  $k$ ,  $\lambda_{max} = k^2/2$ . It is also worth noting that the maximum condition stated above does not agree precisely with the condition which provides the maximum output mechanical energy. The maximum output energy (by neglecting the input electric energy change) can be obtained when the dotted area in Figure 5(c) becomes maximum under the constraint of the rectangular corner point tracing on the line (from  $dE$  on the vertical axis to  $-dE/s$  on the horizontal axis). Therefore, the load should be a half of the maximum generative stress and the mechanical energy:  $-[dE - s(dE/2s)](-dE/2s) = (dE)^2/4s$ . In this case, since the input electrical energy is given by  $[\epsilon_0 \epsilon E + d(-dE/2s)] E$ ,

$$\lambda = 1 / 2[(2/k^2) - 1], \quad (11)$$

which is close to the value  $\lambda_{max}$  when  $k$  is small, but has a different value when  $k$  is large, that is predicted theoretically.

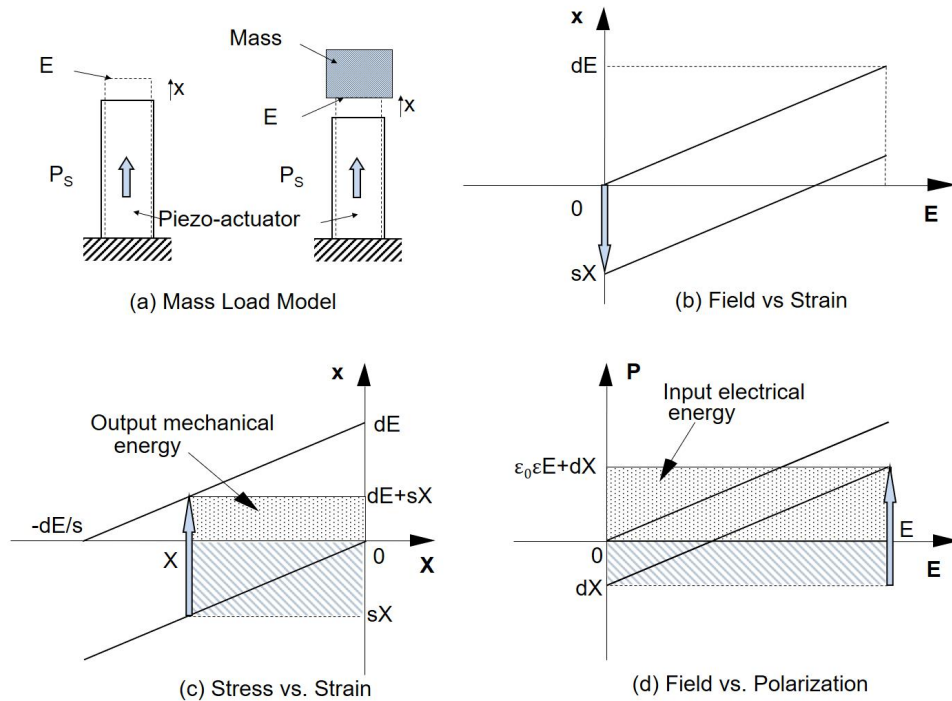


**Figure 5.** Calculation of the input electrical and output mechanical energy: (a) load mass model for the calculation, (b) electric field versus induced strain curve, (c) stress versus strain curve, and (d) electric field versus polarization curve.

### 2.4.3 Efficiency

On the contrary, the efficiency  $\eta$  is defined by

$$\eta = (\text{Output mechanical energy})/(\text{Consumed electrical energy}). \quad (12a)$$

or

$$\eta = (\text{Output electrical energy})/(\text{Consumed mechanical energy}). \quad (12b)$$

If we can recover the mechanically un-consumed energy (stored in the piezoelectric elastic material (*i.e.*, *piezo-spring*)), we can consider that the actually consumed electric energy should be the sum of output mechanical energy (work to the outside) and heat loss, leading to 99% (very high!).

Because the ME researcher may not know how to recover the electrostatic energy stored in the actuator/capacitor, he releases it by shorting the drive circuit in order to move to the next operation. Of course, in this worst scenario, the efficiency less than 25% (equal to  $k^2$ ) is true in his/her paper.

Let us consider how we can recover the electrostatic energy from the piezoelectric capacitor  $[(1 - k^2)$  in the damped capacitance]? Examples can be found in dot-matrix/ink-jet printer and diesel injection valve control applications, where multilayer actuators are driven at  $<1$  kHz, much lower than the resonance frequency. Though the  $k_{33}$  mode is different, refer to a simpler equivalent circuit for the  $k_{31}$  mode shown in **Figure 4(b)** (no-loss case is illustrated). In this equivalent circuit, motional current and damped current ( $C_d = (1 - k^2)C_0$ ) should have  $k^2 : (1 - k^2)$  ratio under an off-resonance condition. If we insert the inductance  $L$  in the driving system so as to create a resonance circuit of  $L$  and  $C_d$  under the condition of  $\omega^2 = 1/LC_d$  ( $\omega$ : operation cycle such as 1 kHz), the electric energy stored in the damped capacitance  $C_d$  starts flip-flopping with  $L$ , without losing this energy (if we neglect the loss or heat generation). When the actuation returns to the original zero-position, the electric energy in the damped capacitance is shifted to the inductor  $L$ , so that the next actuation can start synchronously with the electric energy return to the  $C_d$ . A negative capacitance usage is an alternative solution recently, because the heavy and bulky magnetolectric inductor is problematic for miniaturization.

**Reminder:** (a) Electromechanical coupling factor - *Energy conversion rate*; Energy transmission coefficient - Among the stored mechanical energy  $k^2$  generated by a piezoelectric device, usable mechanical energy is  $1/4 - 1/2$  of the stored energy; Efficiency - The efficiency of the piezoelectric devices is usually high around 99%, if we recover the stored electric energy in a piezo-capacitor with a suitably selected inductance or a negative capacitance. Note, however, the conventional coil inductor kills the size and weight (and Joule loss) in the power supply significantly.

## 2.5 Thin film device designing

**Question 5:** Piezoelectric MEMS (micro electro-mechanical system) is researched popularly with the PZT thin film thickness around  $1 \mu\text{m}$  for the actuators and piezo-energy harvesting applications. What are the major problems to be solved on a popular design shown in **Figure 6**?

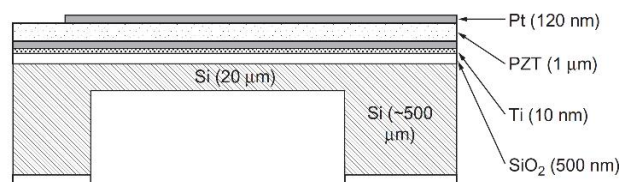


**Figure 6.** Piezoelectric MEMS structure with the PZT thin film thickness around  $1 \mu\text{m}$  for the actuators.

**Solution:** We find two major problems in this design; generative mechanical power level, and PZT and the substrate thickness ratio.

### 2.5.1 Generative mechanical power level

With accelerating the commercialization of piezoelectric actuators and transducers for portable equipment applications, we identified the bottleneck of the piezoelectric devices; that is, significant heat generation limits the maximum power density. Though the problem is much smaller than the EM motors and transformers (*i.e.*, Joule heat from thin conducting wires), the piezo-ceramic devices become ‘ceramic heater’ with increasing the input/output power significantly. When used at its resonance, a piezoelectric device started to generate heat with increasing the vibration level. The vibration velocity, above which  $20^\circ\text{C}$  temperature rise (from room temperature) is observed, is called the “*maximum vibration velocity*” in our community, taking into account the safety to human (*e.g.*, human finger is burned



on a 50°C electronic component!). The current maximum handling power of a well-known hard Pb(Zr,Ti)O<sub>3</sub> (PZT) is only around 10 W/cm<sup>3</sup>. Taking into account the practically required minimum power levels, 30–100 mW for charging electricity into a battery (DC-DC converter spends 2–3 mW), 10–20 mW for soaking blood from a human vessel, or 1–3 mW for sending electronic signal, minimum 1 mW handling is necessary, leading to the minimum PZT volume of 0.1 mm<sup>3</sup>. Only for “nearly-zero” load applications such as optical beam reflectors/mirrors, the power is not very essential unless the agility is required. Accordingly, the MEMS devices with less than 1 μm thin PZT (current commercial base) films are useless from the actuator application view point. 1–10 μW level obtained from 1 μm films is usually used as a ‘sensor’, not as an actuator. At least, 10–30 μm thick films should be used with minimum 3 × 3 mm<sup>3</sup> device area, as long as we use the current existing materials (max power density ~ 10 W/cm<sup>3</sup>). Note that because of the thermal conduction from the silicon substrate, the PZT can be driven under somewhat higher input electrical energy, leading to a higher maximum vibration velocity excited. Thus, the above estimation may be a little pessimistic.

### 2.5.2 PZT/Substrate thickness ratio

A unimorph bending actuator can be fabricated by bonding a piezoceramic plate to a metallic shim, as in **Figure 6**. The tip deflection,  $\delta$ , of the unimorph supported in a cantilever configuration is given by:

$$\delta = \frac{d_{31} E l^2 Y_c t_c}{(Y_m [t_o^2 - (t_o - t_m)^2] + Y_c [(t_o + t_c)^2 - t_o^2])} \quad (13)$$

Here  $E$  is the electric field applied to the piezoelectric ceramic,  $d_{31}$ , the piezoelectric strain coefficient,  $l$ , the length of the unimorph,  $Y$ , Young's modulus for the ceramic or the metal, and  $t$  is the thickness of each material. The subscripts  $c$  and  $m$  denote the ‘ceramic’ and the ‘metal’, respectively. The quantity,  $t_o$ , is the distance between the *strain-free neutral plane* and the bonding surface, and is defined according to the following:

$$t_o = \frac{t_c t_m^2 (3 t_c + 4 t_m) Y_m + t_c^4 Y_c}{6 t_c t_m (t_c + t_m) Y_m} \quad (14)$$

In the case of a unimorph supported at the both two ends, the center displacement is 1/4 of the above displacement. Thus, the analytical approach is the same.

Assuming  $Y_c = Y_m$  just from the simplicity viewpoint, the optimum ( $t_m/t_c$ ) ratio that will maximize the deflection, can be calculated under the following two conditions:

(a) A fixed ceramic thickness,  $t_c$

When we are a purchaser of a PZT plate, we need to find the standard PZT thickness from the company catalogue. Setting  $Y_c = Y_m$ , **Eqs. (13)** and **(14)** become:

$$\delta = \frac{d_{31} E l^2 t_c}{([t_o^2 - (t_o - t_m)^2] + [(t_o + t_c)^2 - t_o^2])} \quad (15)$$

$$t_o = \frac{t_c t_m^2 (3 t_c + 4 t_m) + t_c^4}{6 t_c t_m (t_c + t_m)} \quad (16)$$

Substituting  $t_o$  as it is expressed in **Eq. (16)** into **Eq. (15)** yields

$$\delta = \frac{d_{31} E l^2 3 t_m t_c}{(t_m + t_c)^3} \quad (17)$$

The function  $f(t_m) = (t_m t_c) / (t_m + t_c)^3$  must be maximized for a fixed ceramic thickness,  $t_c$ .

$$\frac{df(t_m)}{dt_m} = \frac{(t_c - 2 t_m) t_c}{(t_m + t_c)^4} = 0 \quad (18a)$$

The metal plate thickness should be  $t_m = t_c/2$  and  $t_o = t_c/2$ .

(b) A fixed total thickness,  $t_c + t_m$

This condition is required when you need to keep the resonance frequency almost constant too keep the tone level, for example, you are a sounder/speaker manufacturer. **Eq. (17)** becomes under a fixed total thickness,  $t_{tot} = t_c + t_m$ :

$$\frac{df(t_m)}{dt_m} = \frac{(t_{tot} - 2t_m)}{t_{tot}^3} = 0 \quad (18b)$$

Thus, it is determined that both the metal and ceramic plate thickness should be  $t_m = t_c = t_{tot}/2$  and  $t_o = t_{tot}/3$ .

Anyhow, in order to obtain the effectively large displacement, the silicon substrate thickness should be in a similar dimension to the PZT thickness. Muralt calculated electromechanical coupling factor  $k$  and the resonance frequency for PZT thin films on a silicon substrate as a function of the substrate thickness on an ultrasonic stator of circular geometry (radius: 5.2 mm, mode B01, PZT with  $e_{31,f}$  of  $-6 \text{ C/m}^2$ ) without considering the film stresses (**Figure 7**)<sup>[7]</sup>. You can find that the electromechanical coupling shows the maximum when the silicon thickness is equal to the PZT thickness.

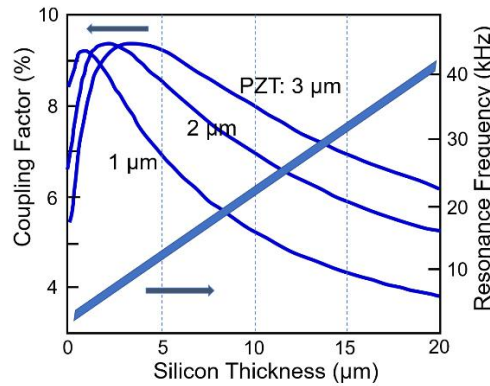
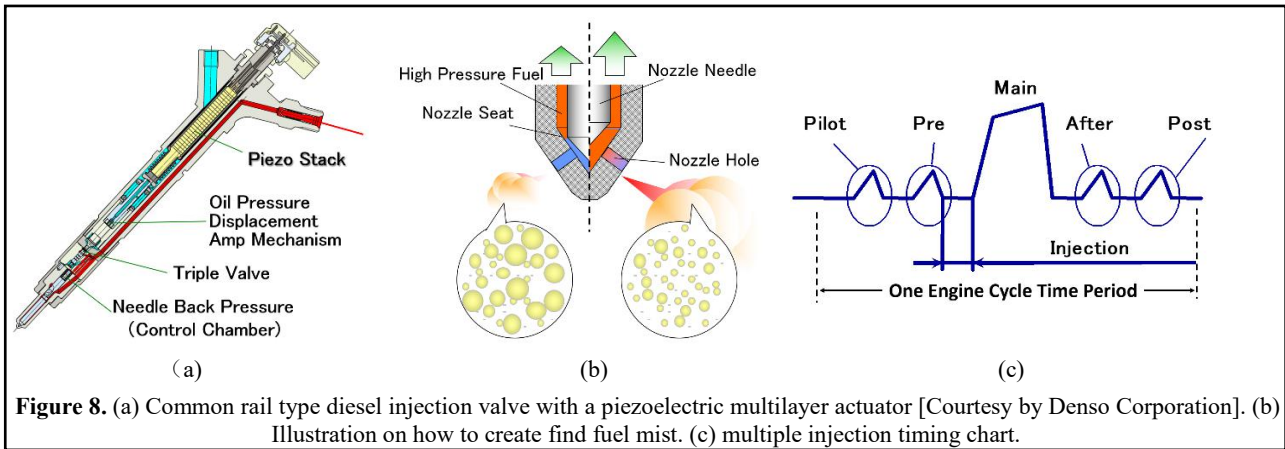


**Figure 7.** Calculated electromechanical coupling factor  $k$  and the resonance frequency for an PZT film ultrasonic circular stator as a function of silicon thickness<sup>[7]</sup>.

**Reminder:** (a) From the generative mechanical power viewpoint (minimum 1 mW), the PZT thickness should be higher than 30  $\mu\text{m}$ . (b) Silicon substrate thickness should be chosen in a similar range of the PZT thickness. PZT 1  $\mu\text{m}$  on 20  $\mu\text{m}$  silicon membrane design published in **Figure 6** may be used for sensor applications, but far from the actuator designs.

## 2.6 Piezoelectric vibration damping

**Question 6:** Because of too fast response of a piezoelectric actuator is, the vibration ringing occasionally follows after the initial response in positioner and pulse drive applications. This problem is experienced during the development of inkjet printers and diesel injection valves. Since the conventional diesel engine requires very fine fuel mist for burning perfectly, new diesel injection valves were developed by Siemens, Bosch and Toyota with piezoelectric multilayered (ML) actuators. **Figure 8(a)** shows such a common rail type diesel injection valve with a ML piezo-actuator, which produces high pressure fuel and quick injection control (7-time open/close valve operations per one engine cycle of 10 msec) (**Figures 8(b)** and **8(c)**)<sup>[8]</sup>. The piezo-actuator's quick response is namely the key to increase burning efficiency and minimize the toxic exhaust gas generation. However, the ringing of the valve rod did not stop easily because of the 10  $\mu\text{sec}$  level response of the ML, so that these additional fuel injections were a serious problem. Automobile engineers tried to install mechanical dampers such as plate springs to suppress the vibration ringing initially, but these also suppressed the displacement amplitude significantly. Provide an piezo-drive idea to suppress the vibration ringing without losing the efficiency like a mechanical damper.



**Solution:** The *Pulse Drive technique* proposed by the author was highly acknowledged to solve the ringing problem by keeping the same (even larger) displacement of the MLs<sup>[9,10]</sup>.

### 2.6.1 Longitudinal vibration through ( $d_{31}$ ) in a rectangular plate

Let us consider the simplest model of the longitudinal mechanical vibration in a piezo-ceramic plate with thickness  $b$ , width  $w$  and length  $L$  ( $b \ll w \ll L$ ), as shown in **Figure 9**. If the polarization is in the  $z$  direction and the  $x$ - $y$  planes are the planes of the electrodes, the extensional vibration in the  $x$  direction is represented by the following dynamic equation:

$$\rho(\partial^2 u / \partial t^2) = F = (\partial X_{11} / \partial x) + (\partial X_{12} / \partial y) + (\partial X_{13} / \partial z), \quad (19)$$

where  $u$  is the displacement of a small volume element in the ceramic plate in the  $x$  direction. When the plate is very long and thin, the longitudinal stresses,  $X_2$  and  $X_3$  may be set equal to zero throughout the plate, and shear stress is not generated by the electric field  $E_z$ , the necessary piezoelectric equation is reduced to:

$$X_1 = x_1 / s_{11}^E - (d_{31} / s_{11}^E) E_z. \quad (20)$$

Thus, we obtain the following dynamic equation (Note that this equation does not include a loss during vibration):

$$\rho(\partial^2 u / \partial t^2) = (1 / s_{11}^E) (\partial^2 u / \partial x^2). \quad (21)$$

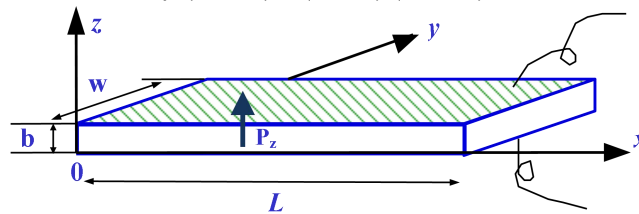


**Figure 9.** Longitudinal vibration through the transverse piezoelectric effect ( $d_{31}$ ) in a rectangular plate ( $L \gg w \gg b$ ).

The differential equation **Eq. (21)** is solved using the *Laplace transform* for the transient response (We will adopt the Fourier transform in the next section for analyzing the steady resonance mode). Denoting the Laplace transforms of  $u(t,x)$  and  $E_z(t)$  as  $U(s,x)$  and  $\tilde{E}(s)$ , respectively, **Eq. (21)** is transformed to:

$$\rho s_{11}^E s^2 U(s,x) = \partial^2 U(s,x) / \partial x^2. \quad (22)$$

This assumes the following initial conditions:

$$u(t=0,x) = 0, \quad \partial u(t=0,x) / \partial t = 0.$$

Using  $\rho s_{11}^E = 1/v^2$  ( $v$ : sound velocity in the piezo-ceramic), we obtain a general solution:

$$U(s,x) = A e^{(sx/v)} + B e^{-(sx/v)}. \quad (23)$$

The constants  $A$  and  $B$  can be determined by the boundary conditions  $X_1=0$  at  $x=0$  and  $L$ . Note that the strain  $x_1$  at  $x=0$  and  $L$  may not need to be zero!:

$$X_1 = (x_1 - d_{31} E_z) / s_{11}^E = 0. \quad (24)$$

Using the fact that the strain  $x_1 = \partial u / \partial x$ ,

$$L[x_1] = \partial U / \partial x = A (s/v) e^{(sx/v)} - B (s/v) e^{-(sx/v)}, \quad (25)$$

the boundary conditions provide the following relations to determine A and B:

$$\begin{aligned} A (s/v) - B (s/v) &= d_{31} \tilde{E}, \\ A (s/v) e^{(sL/v)} - B (s/v) e^{-(sL/v)} &= d_{31} \tilde{E}. \end{aligned}$$

Consequently, **Eqs. (23)** and **(25)** become

$$U(s, x) = d_{31} \tilde{E} (v/s) [(e^{-s(L-x)/v} + e^{-s(L+x)/v} - e^{-sx/v} - e^{-s(2L-x)/v}) / (1 - e^{-2sL/v})], \quad (26)$$

$$L[x_1] = d_{31} \tilde{E} [(e^{-s(L-x)/v} - e^{-s(L+x)/v} + e^{-sx/v} - e^{-s(2L-x)/v}) / (1 - e^{-2sL/v})]. \quad (27)$$

The inverse Laplace transforms of **Eqs. (26)** and **(27)** now provide the displacement  $u(t, x)$  and strain  $x_1(t, x)$ . Since  $u(t, x=L/2) = 0$  [from  $U(s, x=L/2) = 0$ ] and  $u(t, x=0) = -u(t, x=L)$  [from  $U(s, x=0) = -U(s, x=L)$ ], the total displacement of the plate device  $\Delta L$  becomes equal to  $2 u(t, x=L)$ .

$$\begin{aligned} U(s, x=L) &= d_{31} \tilde{E} (v/s) (1 - e^{-(sL/v)}) / (1 + e^{-(sL/v)}) \\ &= d_{31} \tilde{E} (v/s) \tanh(sL/2v). \end{aligned} \quad (28)$$

When  $\tilde{E}$  includes the term of  $(1 + e^{-sL/v})$ , the denominator of **Eq. (28)** disappears and the displacement  $u(t, x)$  is not accompanied by the vibration ringing. However, when  $\tilde{E}$  does not include the term of  $(1 + e^{-sL/v})$ , taking into account the expansion series

$$1 / (1 + e^{-sL/v}) = 1 - e^{-sL/v} + e^{-2sL/v} - e^{-3sL/v} \dots$$

the strain along the  $x$  direction,  $x_1(t, x)$ , is obtained by superimposing the  $d_{31}E_z(t)$  curves with a specific time delay, and the ringing of the displacement will continue forever. This principle is the key to eliminate the unnecessary vibration ringing.

## 2.6.2 Displacement response to a step voltage

We consider first the most fundamental input of *Heaviside step* electric field  $E(t) = E_0 H(t)$ . Since the Laplace transform of the step function is given by  $(1/s)$ , **Eq. (28)** can be expressed by

$$\begin{aligned} U(s, x=L) &= d_{31} E_0 (v/s^2) (1 - e^{-(sL/v)}) / (1 + e^{-(sL/v)}) \\ &= d_{31} E_0 (v/s^2) (1 - 2e^{-(sL/v)} + 2e^{-(2sL/v)} - 2e^{-(3sL/v)} + 2e^{-(4sL/v)} \dots). \end{aligned} \quad (29)$$

Note that the base function of  $U(s, L)$ ,  $1/s^2$ , gives the base function of  $u(t, L)$  in terms of  $t$  (*i.e.*,  $\propto t$ ). The inverse Laplace transform of **Eq. (29)** yields (by superposing the  $e^{-sk}$  terms):

$$\begin{aligned} u(t, L) &= d_{31} E_0 v \cdot t & 0 < t < L/v \\ u(t, L) &= d_{31} E_0 v [t - 2(t - L/v)] & L/v < t < 2L/v \\ u(t, L) &= d_{31} E_0 v [t - 2(t - L/v) + 2(t - 2L/v)] & 2L/v < t < 3L/v \\ u(t, L) &= d_{31} E_0 v [t - 2(t - L/v) + 2(t - 2L/v) - 2(t - 3L/v)] & 3L/v < t < 4L/v \\ &\dots \dots \dots & \dots \dots \dots \end{aligned} \quad (30)$$

The transient displacement,  $\Delta L (= 2u(t, L))$ , produced by the step voltage is pictured in **Figure 10** (since  $d_{31}$  is usually negative, **Figure 10** is for  $E_0 < 0$ ). The resonance period of this piezoelectric plate corresponds to  $(2L/v)$ , and the time interval in **Eq. (30)** is every  $(T/2)$ . It is worth to note that the displacement changes linearly, not sinusoidally. This linear displacement change is originated from the fact that the “step” function strain boundary (*i.e.*, the boundary between the zero strain and maximum strain parts) moves with the sound velocity speed.

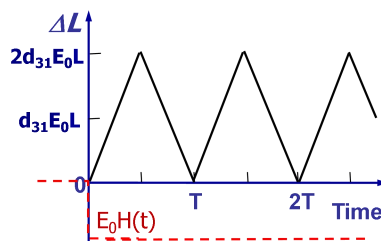


**Figure 10.** Triangular displacement response to a Heaviside step function voltage in a continuum piezoelectric plate ( $d_{31}$  mode).

### 2.6.3 Displacement response to pulse drive

We consider next the response to a rectangular pulse voltage such as pictured in the top left-hand corner of **Figure 11(a)**. We begin by substituting

$$\tilde{E} = (E_0 / s) (1 - e^{-(n s L)/v}) \quad (31)$$

into **Eq. (28)**, which allows us to obtain the displacement  $\Delta L$  for  $n = 1, 2$  and  $3$ . The quantity  $n$  is a time scale based on a half of the resonance period ( $= T/2$ ) of the piezoelectric plate.

**For  $n=1$ ,**

$$\begin{aligned} U(s, x=L) &= d_{31}E_0 (v/s^2) (1 - e^{-(sL/v)})^2 / (1 + e^{-(sL/v)}) \\ &= d_{31}E_0 (v/s^2) (1 - 3e^{-sL/v} + 4e^{-2sL/v} - 4e^{-3sL/v} + \dots). \end{aligned} \quad (32)$$

Similar to the step case, the base function of  $U(s, L)$ ,  $1/s^2$ , gives the base function of  $u(t, l)$  in terms of  $t$ . The inverse Laplace transform of **Eq. (32)** yields:

$$\begin{aligned} u(t, L) &= d_{31}E_0 v \quad t & 0 < t < L/v \\ u(t, L) &= d_{31}E_0 v [t - 3(t - L/v)] & L/v < t < 2L/v \\ u(t, L) &= d_{31}E_0 v [t - 3(t - L/v) + 4(t - 2L/v)] & 2L/v < t < 3L/v \\ & \dots \dots \dots & \dots \dots \dots \end{aligned} \quad (33)$$

The transient displacement,  $\Delta L$ , produced by the rectangular pulse voltage is pictured in **Figure 11(a)** for  $n=1$ . The resonance period of this piezoelectric plate corresponds to  $(2L/v)$ . Notice how continuous ringing occurs under this condition.

**For  $n=2$ ,** since  $\tilde{E} = (E_0 / s) (1 - e^{-(2Ls)/v})$  includes the denominator of **Eq. (5.99)**,

$$U(s, L) = d_{31}E_0 (v/s^2) (1 - 2e^{-sL/v} + e^{-2sL/v}). \quad (34)$$

Thus,

$$\begin{aligned} u(t, L) &= d_{31}E_0 v \quad t & 0 < t < L/v \\ u(t, L) &= d_{31}E_0 v [t - 2(t - L/v)] & L/v < t < 2L/v \\ u(t, L) &= d_{31}E_0 v [t - 2(t - L/v) + (t - 2L/v)] = 0 & 2L/v < t < 3L/v \end{aligned} \quad (35)$$

In this case, the displacement,  $\Delta L$ , occurs in a single pulse and does not exhibit ringing as depicted in **Figure 11(a) Bottom-Left**. Remember again that the applied field  $\tilde{E}$  should include the denominator term  $(1 + e^{-sL/v})$  to realize finite expansion terms, leading to a complete suppression of vibrational ringing.

**For  $n=3$ ,**  $U(s, L)$  is again expanded as an infinite series:

$$\begin{aligned} U(s, x=L) &= d_{31}E_0 (v/s^2) (1 - e^{-(3sL/v)})(1 - e^{-(sL/v)}) / (1 + e^{-(sL/v)}) \\ &= d_{31}E_0 (v/s^2) (1 - 2e^{-sL/v} + 2e^{-2sL/v} - 3e^{-3sL/v} + 4e^{-4sL/v} - 4e^{-5sL/v} \dots). \end{aligned} \quad (36)$$

The displacement response for this case is pictured in **Figure 11(a) Bottom-Right**. Note the displacement slope (plate edge vibration velocity) has twice difference among the field applied period and zero field.

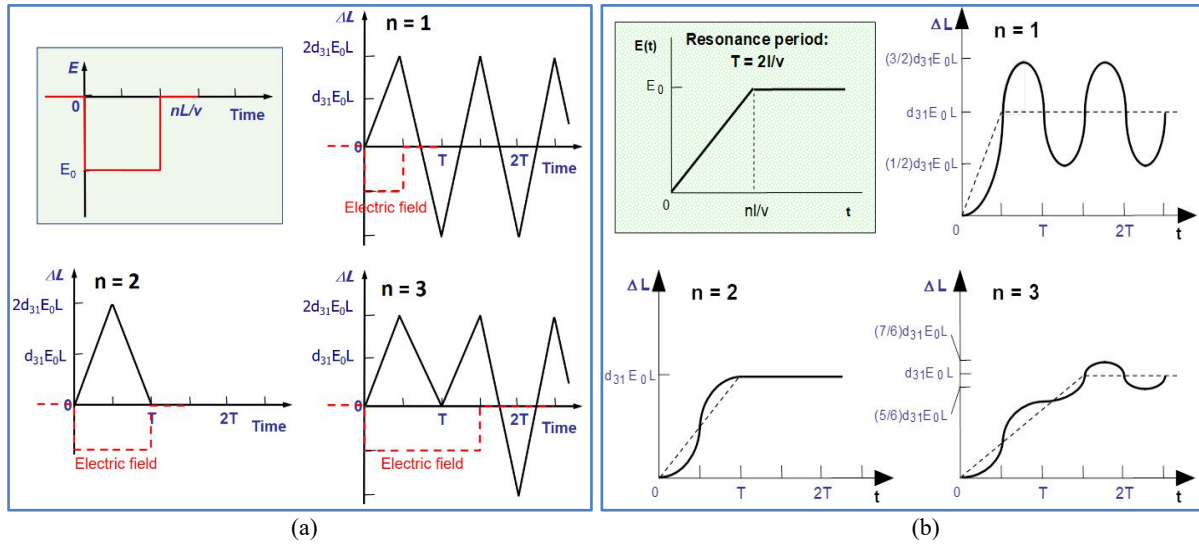


**Figure 11.** Transient displacement  $\Delta L$  induced in a rectangular plate by a rectangular pulse voltage (a), and by a pseudo-step voltage (b). The time scale  $n$  is based on  $1/2$  of the resonance period  $T$ .

### 2.6.4 Displacement response to pseudo-step voltage

Another intriguing wave shape is a pseudo-step shown in **Figure 11(b)**. Substitution of

$$\tilde{E} = (E_0 v / n L s^2) (1 - e^{-snL/v}) \quad (37)$$

into **Eq. (28)**, we obtain the displacement  $\Delta L$  for  $n = 1, 2, 3, \dots$

(1)  $n = 1$ :

$$U(s,L) = (d_{31}E_0 / L) (v^2/s^3) (1 - e^{-sL/v}) / (1 + e^{-sL/v}) \\ = (d_{31}E_0/L)(v^2/s^3)(1 - 3e^{-sL/v} + 4e^{-2sL/v} - 4e^{-3sL/v} + \dots). \quad (38)$$

Note that the base function of  $U(s,L)$ ,  $1/s^3$ , gives the base function of  $u(t,L)$  as  $t^2/2$  (parabolic curve). Thus, considering that the exponential term in the Laplace  $s$  domain corresponds to the time shift in the real time domain [for example,  $e^{-2sL/v}$  in **Eq. (38)** corresponds to the time shift of  $2L/v$  of the base  $u(t,L)$  curve  $t^2$ , that is,  $(t - 2L/v)^2$ ],

$$u(t,L) = (d_{31}E_0v^2/2L) t^2 \quad [0 < t < L/v] \\ u(t,L) = (d_{31}E_0v^2/2L) [t^2 - 3(t - L/v)^2] \quad [L/v < t < 2L/v] \\ u(t,L) = (d_{31}E_0v^2/2L) [t^2 - 3(t - L/v)^2 + 4(t - 2L/v)^2] \quad [2L/v < t < 3L/v] \\ \dots\dots\dots$$

**Figure 11(b) Top-Right** shows the change of  $\Delta L (=2u(t,L))$  with time, which exhibits continuous ringing. Notice that this curve is a combination of parabolic curves, not a sinusoidal curve. The height of the overshoot is  $1/2$  of  $d_{31}E_0L$ .

(2)  $n = 2$ :

$$U(s,L) = (d_{31}E_0 / 2L) (v^2/s^3) (1 - 2e^{-sL/v} + e^{-2sL/v}). \quad (39)$$

Thus,

$$u(t,L) = (d_{31}E_0v^2/4L) t^2 \quad [0 < t < L/v] \\ u(t,L) = (d_{31}E_0v^2/4L) [t^2 - 2(t - L/v)^2] \quad [L/v < t < 2L/v] \\ u(t,L) = (d_{31}E_0v^2/4L) [t^2 - 2(t - L/v)^2 + (t - 2L/v)^2] = d_{31}E_0L/2 \quad [2L/v < t]$$

$\Delta L$  does not exhibit ringing, as shown in **Figure 11(b) Bottom-Left**. When the applied field  $\tilde{E}$  includes the term  $(1 + e^{-sL/v})$ , the expansion series terminates in finite terms, leading to a complete suppression of vibrational ringing.

For  $n = 3$ ,  $U(s,L)$  is expanded again infinitely (*i.e.*, the ringing does not stop). **Figure 11(b) Bottom-Right** shows the displacement change with time. Note again that all the curves are composed of parabolic curves and that the height of



the overshoot is  $1/6$  of  $d_{31}E_0L$ . For  $n = 4$ , you can eliminate the ringing again, because you can imagine that the denominator of the Eq. (28) disappears.

**Reminder:** When  $\tilde{E}$  includes the term of  $(1 + e^{-(sL/n)})$ , the denominator of Eq. (28) disappears and the displacement  $u(t,x)$  is not accompanied by the vibration ringing. An empirical process on how to suppress the overshoot and ringing: (1) By applying a relative steep “step” voltage to the actuator, we can obtain the resonance period from the time period between the overshoot peak and the successive peak point. (2) By adjusting the voltage rise time exactly to the resonance period next time, we can eliminate the overshoot and ringing of the vibration. This vibration ringing suppression technique is not a popular passive (spending the converted electric power via Joule heat) or an active vibration damping (applying the electric power externally to cancel the mechanical vibration), nor dissipates any energy to the outside.

## 2.7 Mechanical impedance matching

**Question 7:** In order to damp a single mode of vibration in an aluminum cantilever beam, a mechanical engineer uses a shunted soft-piezoelectric composite (Macro Fiber Composite by Smart Material Corp., FL) bonded on the beam. This design is NOT an ideal design from the mechanical/acoustic impedance matching. Discuss the problem, and provide an alternative design.

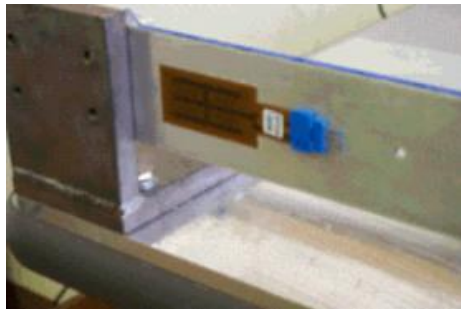


**Figure 12.** Vibration damping of a single mode vibration of an aluminum cantilever beam using a piezoelectric composite bonded on the beam.

### 2.7.1 Mechanical impedance matching

The mechanical work transferred from one object to the other is evaluated by the product of the applied force  $F$  on the interface and the displacement  $\Delta L$  of this interface:

$$W = F \cdot \Delta L \quad (40)$$

**Figure 13(a)** shows a conceptual cartoon illustrating two extreme cases. If the object is very soft, the force  $F$  can be very small, leading to very small  $W$  (practically no work!)[2,3]. This corresponds to “Pushing a curtain,” exemplified by the case when the acoustic wave is generated in water directly by a hard PZT transducer. Most of the acoustic energy generated in the PZT is reflected at the interface, and only a small portion of acoustic energy transfers into water. On the other hand, if the object is very hard, the displacement will be very small, again leading to very small  $W$ . This corresponds to “Pushing a wall.” Polymer piezoelectric PVDF (polyvinylidene di-fluoride) or soft MFC in **Figure 12** cannot drive a hard metal part efficiently. Therefore, the *mechanical/acoustic impedance*  $Z = \sqrt{\rho c}$  must be adjusted to maximize the output mechanical power:

$$\sqrt{\rho_1 c_1} = \sqrt{\rho_2 c_2}, \quad (41)$$

where  $\rho$  is the density and  $c$  is the elastic stiffness, and the subscripts 1 and 2 denote the two materials. This is one of the key factors for developing piezoelectric energy harvesting systems. In practice, in a medical array transducer as shown in **Figure 13(b)**, *acoustic impedance matching layers* (elastically intermediate materials between PZT and water, such as a polymer) are fabricated on the PZT transducer to optimize the transfer of mechanical energy to water. More precisely the matched acoustic impedance  $Z$  should be chosen as  $\sqrt{Z_1 \cdot Z_2}$ , where  $Z_1$  and  $Z_2$  stand for the acoustic impedances of PZT and human tissue (close to water), respectively.

## 2.7.2 Vibration damping and electromechanical coupling

The unimorph piezoelectric element shown in **Figure 12** is a typical example of a combination of a vibration object and a piezoelectric material. The cantilever beam is hit by an impulse force, and the transient vibration displacement decay is monitored by a non-contact displacement sensor.

Let us evaluate the damping constant theoretically<sup>[11]</sup>. The electric energy  $U_E$  generated can be expressed by using the electromechanical coupling factor  $k$  and the input mechanical energy  $U_M$  from the vibration cantilever beam:

$$U_E = U_M \times k^2 . \quad (42)$$

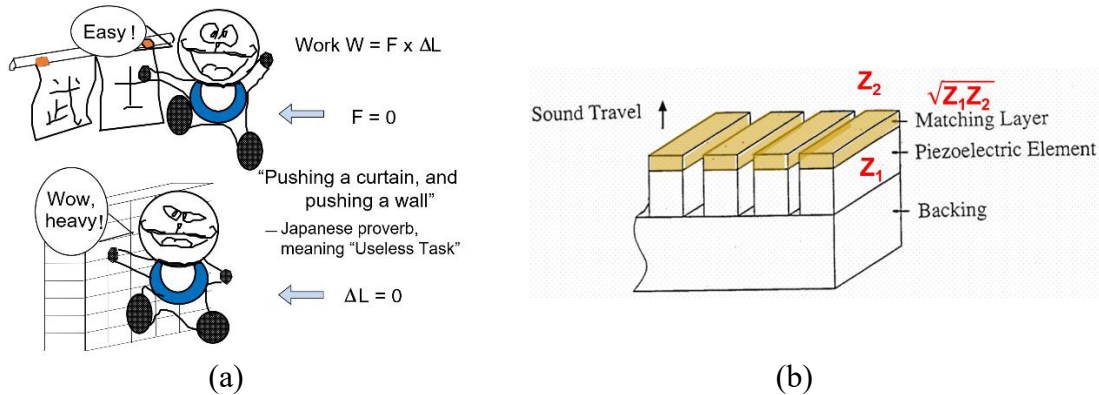


**Figure 13.** (a) Concept of mechanical impedance matching. (b) Medical imaging array transducer assembly.

The piezoelectric damper transforms electric energy into heat energy when the external impedance  $R$  is connected, and transforming rate of the damper can be raised to a level of up to 50% when the electrical impedance is matched. That is, the external resistance  $R$  should be adjusted to  $1/\omega C$ , where  $C$  is the capacitance of the piezo-transducer. Accordingly, the vibration energy is transformed at a rate of  $(1 - k^2/2)$  times with energy vibration repeated, since  $k^2/2$  multiplied by the amount of mechanical vibration energy is dissipated as heat energy. As the square of the amplitude is equivalent to the amount of energy, the amplitude decreases at a rate of  $(1 - k^2/2)^{1/2}$  times with every vibration repeated. If the resonance period is taken to be  $T_0$ , the number of vibrations for  $t$  sec is  $2t/T_0$ . Consequently, the amplitude in  $t$  sec is  $(1 - k^2/2)^{t/T_0}$ . If the residual vibration period is taken to be  $T_0$ , the damping in the amplitude of vibration in  $t$  sec can be expressed as follows:

$$(1 - k^2/2)^{t/T_0} = e^{-t/\tau} . \quad (43)$$

Thus, the following relationship for the time constant  $\tau$  of the vibration damping is obtained.

$$\tau = -\frac{T_0}{\ln(1 - k^2/2)} \quad (44)$$

Because the researcher of **Question 7** used a unimorph structure in his study probably due to the simplest geometry, we cannot expect a sufficient damping performance because of a miserably small electromechanical coupling factor  $k$  ( $< 10\%$ ). The multilayer (ML) PZT actuators with  $k_{33} = 70\%$  will be a better alternative choice for this system. Two ML actuators can sandwich the aluminum beam around the cantilever supporting nodal part with a fixed stiff vise. Since the ML actuator has a similar mechanical impedance to the vibrating metal beam, mechanical energy transfer from the beam to the ML devices is smooth. Furthermore, due to the PZT volume in the ML much larger than the MFC composite, handling energy level will be sufficient to this large beam vibration in the level of mechanical energy  $\sim 10$  W.

**Reminder:** "Pushing a curtain, & pushing a wall". We should consider the mechanical/acoustic impedance matching of the actuators to transfer mechanical energy effectively from both material and structural viewpoints.

## 2.8 Piezoelectric energy harvesting

**Question 8:** During seeking the research trends primarily after the 2000s, with referencing a book Ref. [12], as one of the pioneers in the piezoelectric energy harvesting, Uchino feels a sort of frustration on majority of the recent research papers from the following points:

- (1) Though the electromechanical coupling factor  $k$  is the smallest (*i.e.*, the energy conversion rate from the input mechanical to electric energy is the lowest) among various device configurations, the majority of researchers primarily use the ‘unimorph’ or “bimorph” design.
- (2) Though the typical noise vibration is in a much lower frequency range, the researchers measure the amplified resonant response (even at a frequency higher than 1 kHz) and report these unrealistically harvested electric energy.
- (3) Though the harvested energy is lower than 1 mW, which is lower than the required electric energy to operate a typical energy harvesting electric circuit with a DC/DC converter (typically around 2–3 mW), the researchers report the result as an energy ‘harvesting’ system. Does this situation mean actually energy ‘losing’ systems?
- (4) Few papers have reported complete energy flow or exact efficiency from the input mechanical noise energy to the final electric energy in a rechargeable battery via the piezoelectric transducer step by step. In comparison with competitive commercial product solar cells with efficiency 5–9%, the customers of piezo-energy harvesting devices may expect an efficiency of a similar range.

Interestingly, the unanious answer from these researchers to my above questions ‘why?’ is “because the previous researchers did so”. Can you provide the better strategies to answer to the above questions?

**Solution:** Piezoelectric energy harvesting has been receiving a research interest in the 21st century from a sustainability and renewable energy aspect. The author started piezoelectric damping technology in the 1980s, for suppressing the engine noise vibration. However, after the 1990s, cyclic electric field excited in the piezoelectric plate by the environmental noise vibration is accumulated into a rechargeable battery without consuming it just as Joule heat<sup>[13]</sup>. “Lightning Switch”<sup>[13]</sup> (remote switch for room lights, with using a unimorph piezoelectric component) by PulseSwitch Systems, VA is one of the successful million-selling products in the commercial market. In addition to the living convenience, Lightning Switch can reduce the housing construction cost. The 25 mm caliber “Programmable Ammunition” by ATK, AZ and Micromechanics, PA<sup>[13]</sup> uses a multilayer piezo-actuator for generating electric energy under shot impact to activate the operational amplifiers which ignite the burst according to the command program.

Though Uchino is excited by hearing dramatic increase in the research publication in this field, he is partially embarrassed with reading ridiculous publications such as:

- Energy harvesting from a hard steel structure with a soft piezo-material – Mechanical impedance mismatch.
- Energy harvesting from a high frequency (100 kHz) resonant state – Natural noise is not of this high frequency.
- Miserably small energy harvesting ( $\mu\text{W}$ ) from MEMS structure – Harvesting circuit consumes mW!

The author describes here the initial research guidelines and bring in light the problems and limitations of implementing the piezoelectric transducer. The Penn State group developed energy harvesting piezoelectric devices based on a “Cymbal” structure (29 mm $\phi$ , 1-2 mm thick), which can generate electric energy up to 100 mW under an automobile engine vibration<sup>[14,15]</sup>. By combining three cymbals in a rubber composite, a washer-like energy harvesting sheet was developed for a hybrid car application, aiming at 1W-level constant accumulation from the engine vibration to a fuel cell. There are three major phases/steps associated with piezoelectric energy harvesting, as described in **Figure 14**<sup>[13]</sup>: (i) *mechanical-mechanical energy transfer*, including mechanical stability of the piezoelectric transducer under large stresses, and mechanical impedance matching, (ii) *mechanical-electrical energy transduction*, relating with the electromechanical coupling factor in the composite transducer structure, and (iii) *electrical-electrical energy transfer*, including electrical impedance matching, such as a DC/DC converter to accumulate the energy into a rechargeable

battery.

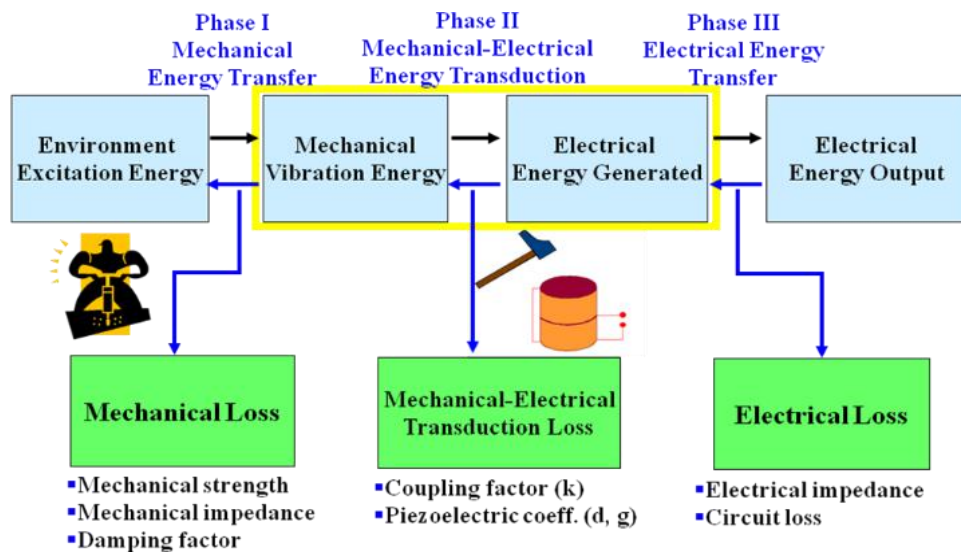


**Figure 14.** Three major phases associated with piezoelectric energy harvesting): (i) mechanical-mechanical energy transfer, (ii) mechanical-electrical energy transduction, and (iii) electrical-electrical energy transfer.

Let us consider how much energy amount decreases under successive transmitting and transducing phases by numerical analyses through **Figure 15**. The sample used here is a cymbal with 0.3 mm-thick stainless-steel endcaps, inserted below a 4 kg engine weight (*i.e.*, 40 N bias force). The electromagnetic shaker was operated at 100 Hz (*i.e.*, actual engine noise frequency) for 8 seconds, and the accumulated energy during that time period was measured at each point.

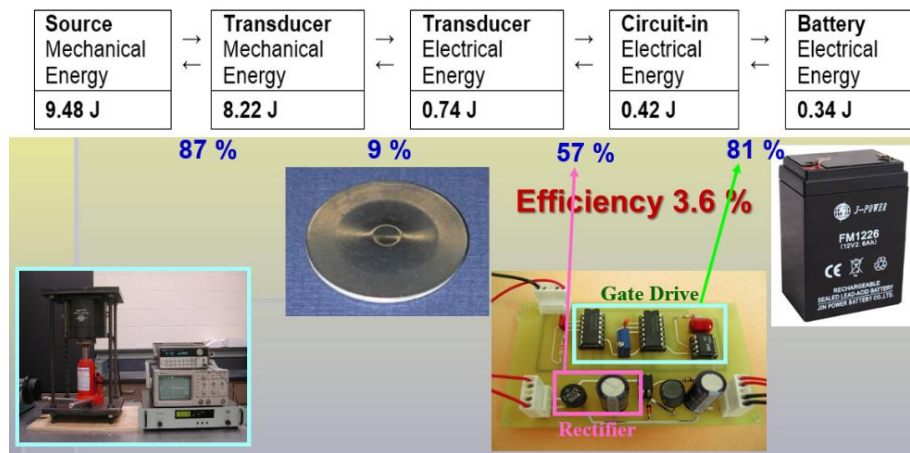


**Figure 15.** Energy flow analysis from the vibration source, through the piezoelectric element, then via energy harvesting circuits, to finally into a rechargeable battery.

### 2.8.1 Source to transducer: mechanical impedance mismatch

$8.22 \text{ J}/9.48 \text{ J} = 87\%$  of the mechanical energy is transmitted from the source to piezo-cymbal transducer. If the mechanical impedance is not seriously considered in the transducer (too mechanical-soft or hard), the mechanical energy will not transfer efficiently, and large amount will be reflected at the contact/interface point.

### 2.8.2 Transduction in the transducer: electromechanical coupling

Transduction rate is evaluated by  $k^2$ . Since the  $k_{eff} = 0.25\sim 0.30$  in the cymbal, the energy conversion rate will be 9% maximum. The remaining portion will remain as the original mechanical vibration energy.  $0.74 \text{ J}/8.22 \text{ J} = 9.0\%$ . Since

$k_{eff}$  of the bimorph or unimorph is much smaller (10~15%), the energy conversion rate is smaller than 2%. Using transducer modes with higher  $k$  values is highly recommended.

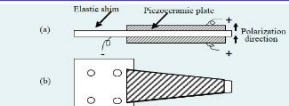
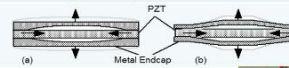
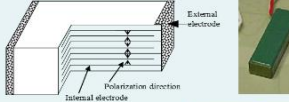
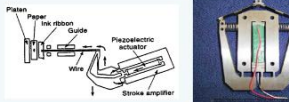
### 2.8.3 Transducer to harvest circuit: electrical impedance matching

$0.42 J / 0.74 J = 57\%$  is related with the electrical impedance mismatch between the cymbal output and the circuit input. The AC/DC rectifying circuit is the major cause of a half cut.

### 2.8.4 Harvesting circuit to rechargeable battery

$0.34 J / 0.42 J = 81\%$ . This reduction is partially originated from the energy consumption in the circuit, and partially originated from the electrical impedance mismatch between the circuit output (still around  $5 k\Omega$ ) and the rechargeable battery impedance (around  $10-20 \Omega$ ). Since a circuit consumes  $1-3 mW$  normally, the energy harvesting less than  $mW$  is useless.

As the reader already recognized, the major problem in the piezoelectric energy harvesting is the low electromechanical coupling factor used by the researchers. If we adopt the ML type actuator with  $k_{33} = 50\%$ , we can enhance the efficiency by 10 times. Refer to **Figure 16**.

Device Design	$k_{eff}$ (%)	Response
<b>Unimorph/ Bimorph</b> 	10%	0.5 – 2 kHz
<b>Moonie/ Cymbal</b> 	30%	10 – 40 kHz
<b>Multilayer</b> 	70%	50 – 300 kHz
<b>Multilayer + Hinge Lever</b> 	70%?	1 – 20 kHz

**Figure 16.** Promising piezoelectric device designs for energy harvesting applications.

**Reminder:** Unimorph/bimorph configurations are not recommended for the piezo-energy harvesting system (too low  $k$ ). Do not argue the energy harvesting at the resonance frequency of the piezo-component (unrealistic value).  $0.34 J / 9.48 J = 3.6\%$  is the current energy harvesting rate from the vibration source to the storing battery. Losses in all the above phases should be taken into account, in order to increase the system efficiency. High  $k$  design is recommended. Regarding the MEMS energy harvesting researchers, you are requested to focus the research on how to parallelly connect thousands of  $\mu W$  components synchronously, so that the total electrical energy would reach to  $mW$ , practically usable level!

## 2.9 Resonance & antiresonance modes

**Question 9:** Materials engineers usually consider, “The resonance mode is only the mechanical resonance, while the antiresonance mode is not a mechanical resonance, because the displacement amplitude of a piezo-specimen enhances only at its resonance frequency, not at the antiresonance frequency, when we drive it under a constant voltage,” or “The resonance mode is the best efficient driving condition of the piezoelectric transducer.” Can the reader recognize the above two claims are from misconceptions on the piezoelectricity?



**Solution:** The resonance/antiresonance vibration modes are basically sinusoidal, and we use Fourier transform, rather than Laplace transform for the continuous and steady vibration analysis. We consider again the longitudinal mechanical vibration of a piezoceramic plate through the transverse piezoelectric effect ( $d_{31}$ ) shown in **Figure 9**. If the polarization is in the z-direction and x-y planes are the planes of the electrodes, the extensional vibration in the x direction is represented by **Eq. (21)** (when the length  $L$  is more than 4~6 times of the width  $w$  or the thickness  $b$ , we can neglect the coupling modes with width or thickness vibrations), leading to a harmonic vibration<sup>[13]</sup>, and

$$-\omega^2 \rho s_{11}^E u = \partial^2 u / \partial x^2. \quad (45)$$

Here,  $\omega$  is the angular frequency of the drive field, and  $\rho$  is the density. Substituting a general solution  $u = u_1(x)e^{j\omega t} + u_2(x)e^{-j\omega t}$  into **Eq. (45)**, and with the boundary condition  $X_l = 0$  at  $x = 0$  and  $L$  (sample length) (due to the mechanically-free condition at the plate end), the following solution can be obtained:

$$\begin{aligned} \partial u / \partial x = x_1 &= d_{31} E_z [\sin \omega(L-x)/v + \sin(\omega x/v)] / \sin(\omega L/v) \\ &= d_{31} E_z \left( \frac{\cos \left[ \frac{\omega(L-2x)}{2v} \right]}{\cos \left( \frac{\omega L}{2v} \right)} \right), \end{aligned} \quad (46)$$

where  $v$  is the *sound velocity* expressed by  $v = 1 / \sqrt{\rho s_{11}^E}$ .

Note that both resonance and antiresonance modes are the “mechanical resonance”. However, electrical engineers focus on the electrical impedance [(applied voltage/induced current) ratio] or admittance from the drive system viewpoint. The current flow into the specimen is described by the surface charge increment,  $\partial D_3 / \partial t$ , and the total current is given by:

$$\begin{aligned} i &= j\omega w \int_0^L D_3 dx = j\omega w \int_0^L (d_{31} X_1 + \epsilon_{33}^X E_z) dx \\ &= j\omega w \int_0^L [d_{31} \{x_1 / s_{11}^E - (d_{31} / s_{11}^E) E_z\} + \epsilon_{33}^X E_z] dx. \end{aligned} \quad (47)$$

Using **Eq. (46)**, the admittance  $Y$  for the mechanically free sample is calculated to be:

$$\begin{aligned} Y = (i/V) &= (i/E_z b) \\ &= (j\omega w L / E_z b) \int_0^L [ (d_{31}^2 / s_{11}^E) \left( \frac{\cos \left[ \frac{\omega(L-2x)}{2v} \right]}{\cos \left( \frac{\omega L}{2v} \right)} \right) E_z + [\epsilon_{33}^X - (d_{31}^2 / s_{11}^E)] E_z ] dx \\ &= (j\omega w L / b) \epsilon_{33}^{LC} [1 + (d_{31}^2 / \epsilon_{33}^{LC} s_{11}^E) (\tan(\omega L / 2v) / (\omega L / 2v))]. \end{aligned} \quad (48)$$

Here,  $w$  is the width,  $L$  the length,  $b$  the thickness of the rectangular piezo-sample, and  $V$  is the applied voltage.  $\epsilon_{33}^{LC}$  is the permittivity in a *longitudinally clamped* sample, which is given by

$$\epsilon_{33}^{LC} = \epsilon_{33}^X - (d_{31}^2 / s_{11}^E). \quad (49)$$

### 2.9.1 Resonance & antiresonance modes

The “piezoelectric resonance” is achieved where the admittance becomes infinite or the impedance is zero (by neglecting material’s losses). Thus, the resonance frequency  $f_R$  is calculated from  $\omega L / 2v = \pi / 2$  in **Eq. (48)**, because  $\tan(\omega L / 2v) \rightarrow \infty$  for  $\omega L / 2v \rightarrow \pi / 2$ . The fundamental frequency is expressed as

$$f_R = \omega_R / 2\pi = v / 2L = 1 / (2L \sqrt{\rho s_{11}^E}). \quad (50)$$

On the other hand, the antiresonance state is generated for zero admittance or infinite impedance. By putting  $Y = 0$  in **Eq. (48)**:

$$(\omega_A L / 2v) \cot(\omega_A L / 2v) = -d_{31}^2 / \epsilon_{33}^{LC} s_{11}^E = -k_{31}^2 / (1 - k_{31}^2). \quad (51)$$

The final transformation is provided by the electromechanical coupling factor definition,

$$k_{31} = d_{31} / \sqrt{s_{11}^E \cdot \epsilon_{33}^X}. \quad (52)$$

The mode difference between the resonance and antiresonance states is described by the following intuitive model. In a high electromechanical coupling material with  $k_{31}$  almost equal to 1, the resonance or antiresonance states appear for  $\tan(\omega L / 2v) = \infty$  or 0 [i.e.,  $\omega L / 2v = (m-1/2)\pi$  or  $m\pi$  ( $m$ : integer)], respectively. The strain amplitude  $x_l$  distribution for each state [calculated using **Eq. (46)**] is illustrated in **Figure 17**. In the resonance state, large strain amplitudes and associated large capacitance changes (called *motional capacitance*) are induced, and the current can easily flow into the device (i.e., large admittance). To the contrary, at the antiresonance, the strain induced in the device compensates completely (due to one wave length), resulting in no dynamic/motional capacitance change, and the current cannot



flow easily into the sample. Thus, for a high  $k$  material the first antiresonance frequency  $f_A$  should be twice as large as the first resonance frequency  $f_R$ . Note that the maximum strain level is in the same magnitude for the resonance and antiresonance modes.

The stress  $X_1$  at the plate ends ( $x = 0$  and  $L$ ) is supposed to be zero in both cases. However, though the strain  $x_1$  at the plate ends is nearly-zero for the resonance, the strain  $x_1$  is not zero for the antiresonance. This means that there is only one vibration node at the plate center for the resonance (**Top-left** in **Figure 17**), and there are additional two nodes at both plate ends for the antiresonance (**Top-right** in **Figure 17**) for  $k_{31} = 1$  (*i.e.*, the end displacement is very small, though the internal plate displacement is large).

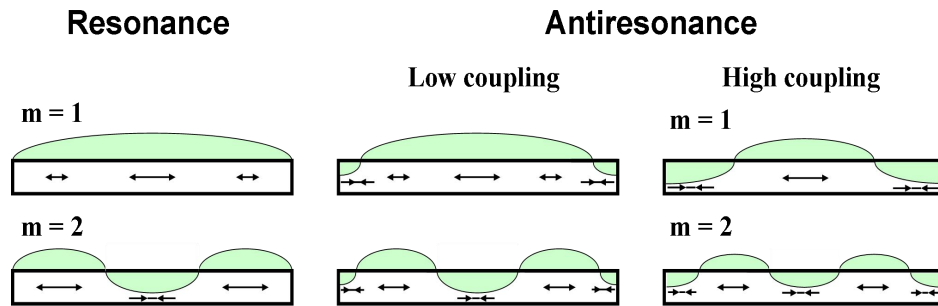


**Figure 17.** Strain distribution in the resonant and antiresonant states.

In a practical PZT case with  $k_{31} = 0.3$ , the antiresonance state varies from the previously-mentioned mode and becomes closer to the resonance mode (**Top-center** in **Figure 17**). This low-coupling material exhibits an antiresonance mode where the capacitance change due to the size change (*motional capacitance*) is compensated completely by the current required to charge up the static capacitance (called *damped capacitance*). Thus, the antiresonance frequency  $f_A$  will approach the resonance frequency  $f_R$ . The displacement at the end is almost the same as the maximum (anti-node) point when  $k_{31}$  is small.

Though both the resonance and antiresonance states are under the mechanical resonance, the misconception that “the antiresonance is not a mechanical resonance” occurs because no displacement enhancement is observed under a *constant voltage drive*. If you notice that the antiresonance state has very high impedance, the current flows minimum (*i.e.*, very low input electric power), leading to low mechanical excitation. If the experiment is made under a *constant current drive*, a huge voltage (*i.e.*, very high power input) is applied at the anti-resonance, leading to the peak vibration level.

In order to verify the mechanical resonance of the antiresonance mode, we explain the *mechanical excitation* of this mode by using a burst/transient method<sup>[16]</sup>. In the *burst method*, the piezo-ceramic is excited for a set number of ac (near resonance) voltage cycles, after which the electrically shut-down, and short-circuit (*i.e.*, resonance under electrical excitation) or open-circuit (*i.e.*, antiresonance under electrical excitation) conditions are imposed on the sample for observing the “mechanical” decaying ac vibration without electrical power input (See **Figure 18**). It is noteworthy that the vibration amplitude and velocity are exactly proportional to current and voltage generated in the piezo-ceramic at the resonance or antiresonance mode, respectively. The decay of current or voltage allows for the calculation of the mechanical quality factors at resonance  $Q_A$  and antiresonance  $Q_B$ , respectively, as a function of vibration velocity, an important figure of merit for high power applications (this methodology will be used in the next **Subsection 2.9.2**). It is important to point out that the mechanical resonance frequency in the vibration velocity monitoring suddenly changes only for the open-circuit condition; that is, the natural “mechanical antiresonance” mode is excited after the burst resonance mode drive!

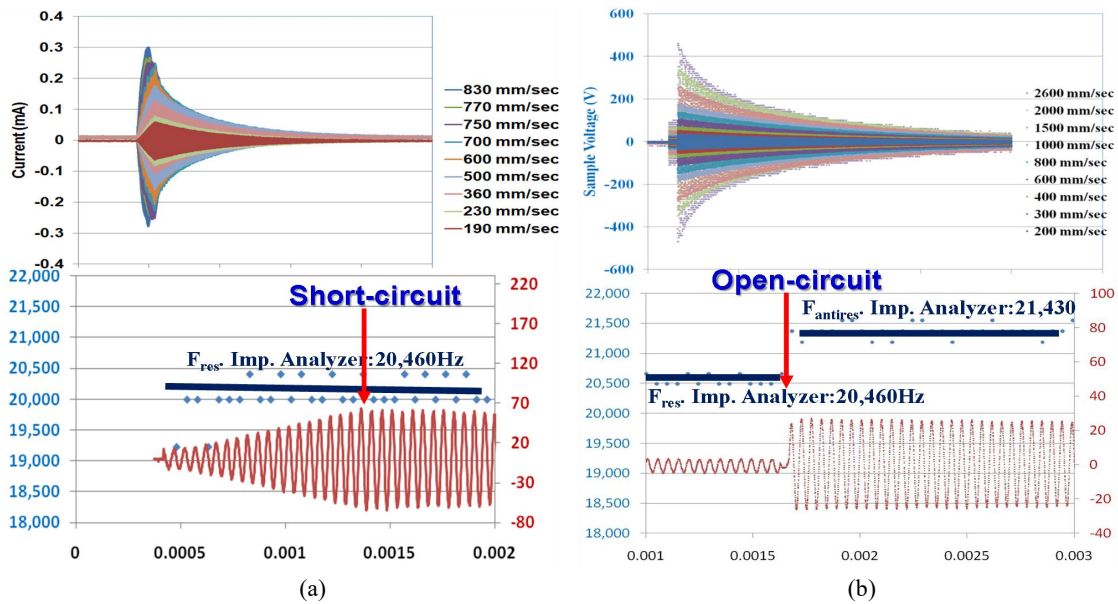


**Figure 18.** (a) Burst methods under short-circuit condition, where current and vibration velocity change proportionally; (b) Burst methods under open-circuit condition, where voltage and vibration velocity change proportionally. Note the resonance frequency jump to the antiresonance frequency for the open-circuit.

## 2.9.2 Heat generation at antiresonance mode

High power piezoelectrics with low loss have become a central research topic from the energy-efficiency improvement viewpoint; that is to say, the research focus is shifting from “real (off-resonance strain magnitude)” to “imaginary performance (heat generation reduction)”. Reducing hysteresis and increasing the mechanical quality factor to amplify the “resonance displacement” is the primary target from the transducer application viewpoint. Piezoelectric properties change owing to its non-linearity and hysteresis introduced under high excitation conditions. High Power Characterization System (HiPoCS™) was developed in the ICAT (Penn State) to fill the void between initial property measurements under small vibration velocity and actual service conditions under high vibration velocity with heat generation<sup>[17]</sup>. HiPoCS is capable of measuring high power characteristics and imitate service conditions of piezoelectric materials under constant voltage ( $V_{rms}$ ), current ( $A_{rms}$ ), vibration velocity ( $V_{rms}$ ), and input electrical power ( $P_i$ ) modes. Previous measurements under constant voltage or current modes cannot provide the precise mechanical quality factors  $Q_A$  and  $Q_B$  from the admittance/impedance curves because of a significant distortion (*i.e.*, skewed shape) in the spectra due to the elastic non-linearity of the piezo-ceramics. Therefore, the major advancement in high power measurement was brought by the constant vibration velocity mode in HiPoCS. In this mode, the material’s stored mechanical energy level is kept constant throughout the measurement so that the elastic nonlinearities and thus-associated admittance spectrum distortions in property calculations can be avoided.

**Figure 19(a)** shows voltage and current characteristics in the frequency sweep from the resonance to the antiresonance points under constant vibration velocity with HiPoCS, measured on a PZT ceramics. Using the 3 dB up method for the voltage or current curve, the mechanical quality factor at resonance  $Q_A$  or at antiresonance  $Q_B$  can be obtained. It is obvious that the apparent power (the product voltage & current) is smaller at the antiresonance than the resonance under the same output vibration level; that is, the efficiency is higher at the antiresonance than the resonance in the PZTs. The Uchino’s motivation for clarifying the loss mechanisms came up when I realized the significant  $Q_M$  difference between the resonance and antiresonance in the PZT ceramics in the late 1980s, which the IEEE Standard measuring method could not explain at all.

In order to explain the physical background on why the antiresonance mechanical quality factor is larger than that of resonance, a brief loss phenomenology is introduced here. Refer to **Ref. [18]** for the details. There are three losses in

piezoelectrics: dielectric  $\tan \delta$ , elastic  $\tan \phi$ , and piezoelectric  $\tan \theta$ , each of which is further categorized intensive (observable) and extensive (material parameter) losses as defined by:

$$\begin{aligned} \varepsilon^{X*} &= \varepsilon^X (1 - j \tan \delta'), & s^{E*} &= s^E (1 - j \tan \phi'), & d^* &= d (1 - j \tan \theta'); \\ \kappa^{X*} &= \kappa^X (1 + j \tan \delta), & c^{D*} &= c^D (1 + j \tan \phi), & h^* &= h (1 + j \tan \theta). \end{aligned}$$

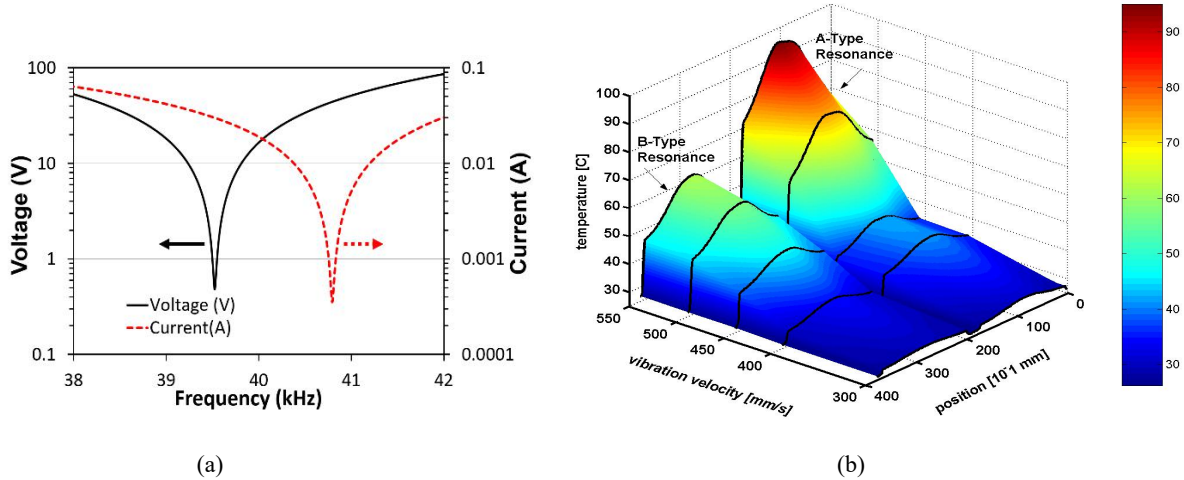


**Figure 19.** (a) Voltage and current characteristics in the frequency sweep from the resonance to the antiresonance frequency under constant vibration velocity with HiPoCS, measure on a PZT ceramics. (b) Heat generation profiles for the resonance (Type A) and antiresonance (Type B) under the same vibration level (*i.e.*, vibration velocity) on a hard PZT (APC 851) with HiPoCS<sup>[17,19]</sup>.

Intensive (prime) and extensive (non-prime) losses correspond to the ‘stress-free or short-circuit’ status and the ‘clamped or open-circuit’ status, respectively. Furthermore, the extensive and intensive loss factors have the following relationship for the  $k_{31}$  mode:

$$\begin{bmatrix} \tan \delta' \\ \tan \phi' \\ \tan \theta' \end{bmatrix} = K \begin{bmatrix} \tan \delta \\ \tan \phi \\ \tan \theta \end{bmatrix} \quad \text{or} \quad \begin{bmatrix} \tan \delta \\ \tan \phi \\ \tan \theta \end{bmatrix} = K \begin{bmatrix} \tan \delta' \\ \tan \phi' \\ \tan \theta' \end{bmatrix}, \quad (53)$$

$$K = \frac{1}{1-k^2} \begin{bmatrix} 1 & k^2 & -2k^2 \\ k^2 & 1 & -2k^2 \\ 1 & 1 & -1-k^2 \end{bmatrix}. \quad (54)$$

The conversion matrix  $K$  (composed of the electromechanical coupling factor  $k$ ) is proven to be *involutory*, *i.e.*  $K^2 = I$ , or  $K = K^{-1}$ , where  $I$  is the identity matrix.

We derived the formula of  $Q_A$  and  $Q_B$  in terms of the three loss factors for various vibration modes in **Ref [18]**. For example,  $k_{31}$ :

$$Q_{A,31} = \frac{\Omega_A}{2\Delta_A} = \frac{1}{\tan \phi_{11}'} \quad (55)$$

$$\frac{1}{Q_{B,31}} = \frac{1}{Q_{A,31}} - \frac{2}{1 + \left(\frac{1}{k_{31}} - k_{31}\right)^2 \Omega_B^2} (2 \tan \theta_{31}' - \tan \delta_{33}' - \tan \phi_{11}') \quad (56)$$

Note here that  $(2 \tan \theta_{31}' - \tan \delta_{33}' - \tan \phi_{11}')$  is a sort of “*electromechanical coupling loss*” term derived from **Eq. (52)**. Though the previous researchers neglected the piezoelectric loss ( $\tan \theta'$ ), we pointed out that piezoelectric loss has the largest magnitude in comparison with the dielectric and elastic losses, and is essential to explain the admittance/impedance spectrum. In order to explain the fact  $Q_A < Q_B$  in PZTs, the piezoelectric loss should be larger than other dielectric and elastic losses ( $2 \tan \theta_{31}' > \tan \delta_{33}' + \tan \phi_{11}'$ ). Note that the empirical rule “ $Q_A < Q_B$ ” is not always true for the Pb-free piezoelectrics. **Figure 19(b)** demonstrates the heat generation profiles on a Hard PZT specimen for the resonance (Type A) and antiresonance (Type B) under the same vibration level drive (*i.e.*, vibration velocity).

Under  $v_{rms} = 0.55$  m/sec, the maximum temperature at the nodal point ( $60^{\circ}\text{C}$ ) under the antiresonance is much lower than that under the resonance ( $95^{\circ}\text{C}$ ), as expected from  $Q_A < Q_B$ .

**Reminder:** In PZTs, the antiresonance mode exhibits better efficiency (lower heat generation) than the resonance mode for generating the same mechanical output in the transducer applications. Just the difference is the drive scheme: high voltage, low current drive for the antiresonance, while low voltage, high current drive for the resonance.

## 2.10 Best-selling devices

**Question 10:** In order to improve the performance of a system, recent researchers tend to add additional components to the original design; for example, in order to upgrade the positioning resolution to 10 nm level on the linear stage with the original resolution 1  $\mu\text{m}$ , an additional motor is integrated to make the control system much more complex. We call this approach as “*Spaghetti Syndrome*”, which is not highly recommended. Most of the researchers also seem to believe that improving the performance is the best way for seeking for the successful “Best-Selling” device. This is actually not true from the industrial or manufacturer’s viewpoint. In collaboration with Samsung Electromechanics, Korea, the ICAT/Penn State developed a zoom/focus camera module for mobile phones with two micro rotary motors (**Figure 20(c)**) in the early 2000s. We had a sophisticated world-smallest motor made of a PZT tube motor, as illustrated in **Figure 20(a)** at that time<sup>[20]</sup>, which was adopted on the cover page of the IEEE Transaction. The “PZT tube type” consists of a PZT hollow cylinder with the radial poling direction. Four-phase (sine, cosine, -sine, -cosine) voltage is applied on the four segmented electrodes on the cylinder surface, so that a ‘wobbling’ vibration is excited on the tube, like a Hula-Hoop motion to drive a rotor. Though the motor performance (rotation speed, torque, power, and size) was satisfactory, the Samsung VP did not adopt this design for their camera module component. Discuss the reasons from the commercialization strategic viewpoint.

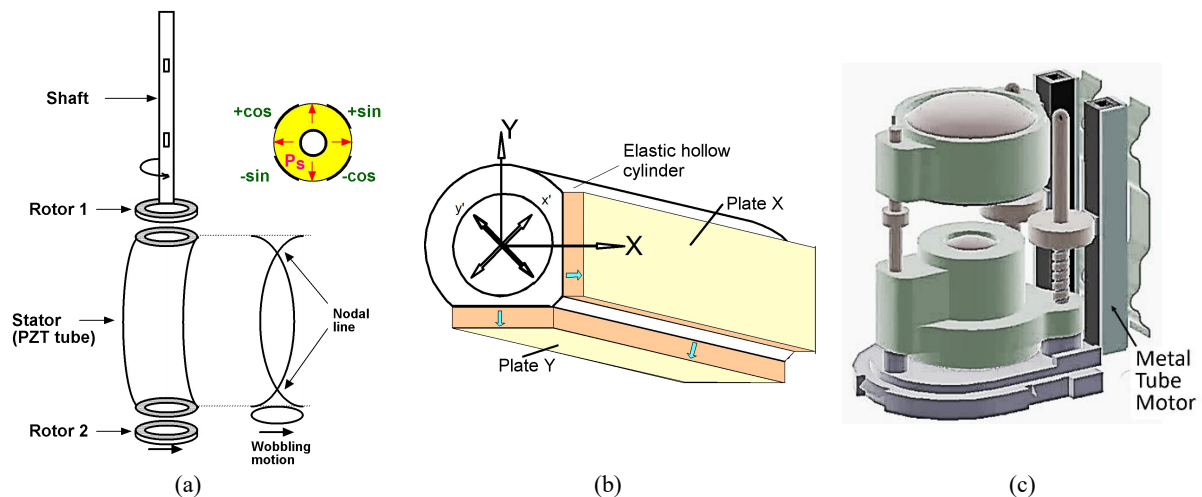


**Figure 20.** (a) PZT tube motor<sup>[20]</sup>, (b) metal tube motor<sup>[21]</sup>, and (c) camera module with two ultrasonic motors.

**Solution:** In the middle 1980s, Akio Morita, former president of SONY Corporation, responded to criticism from a journalist concerning the lack of creativity on the part of Japanese researchers by saying “Japanese researchers are good at chasing and imitating the original idea for commercialization, but they in general lack creativity.” Mr. Morita suggested that there should be three types of creativity with respect to Research & Development at SONY: “The U.S. people are focusing only on *technological creativity*. But the people must understand there are two more creativities; *product planning creativity* and *marketing creativity*, which are equally important for commercial success.”

The rejection of the “PZT tube motor” for the Samsung new camera module application came mainly from the following two problems:

- (1) Cost: PZT rectangular plate (2 ¢) → disk (5 ¢) → ring (10 ¢) → cylinder (40 ¢). Since Samsung was seeking the price target ~ 40 ¢, including the motor and driver, 40 ¢ just for a PZT tube does not match.
- (2) Durability: For a mobile phone application, the durability test (5 G shock test from 2 m height for 1000 times) is required. The PZT tube did not endure this shock test.

Therefore, we developed the “Metal-tube type” consisting of a metal cylinder and two PZT cheap rectangular plates, by sacrificing the motor performance slightly due to the smaller PZT volume (See **Figure 20(b)**)<sup>[21]</sup>. When we drive one of the PZT plates, Plate X, a bending vibration is excited basically along x axis. However, because of an asymmetrical mass (Plate Y), another hybridized bending mode is excited along y axis with some phase lag, leading to an elliptical locus in a clockwise direction (basically similar Hula-Hoop motion to the PZT-tube type)<sup>[21,22]</sup>. The rotor of this motor is a cylindrical rod with a pair of stainless ferrule pressed with a spring. A no-load speed of 1800 rpm and an output torque 1.8 *mN·m* under an applied voltage of 80 *V<sub>rms</sub>* was sufficient for the camera module application (maximum efficiency ~ 28%). We can say that we selected the ‘second-rank’ design just from the *technological creativity* viewpoint.

The author introduces a basic *product planning* strategy/procedure in narrowing the development focus below.

### 2.10.1 List all the possible application fields

When we invented piezoelectric actuators, we considered initially various application fields:

1. Office equipment (Printer, Fax machine)
2. Cameras
3. Automobiles

Can you identify the development “*pecking order*” among these application areas? The author will introduce so-called strategic or managerial decision making procedure in the simplest way, using this practical example.

### 2.10.2 Start with the simplest specifications

Among the possible applications, we tried to find the simplest technological specifications. Basically, we considered restrictions by the International Industrial Standards (IIS), first.

*Temperature range* – The standard temperature requirements for office equipment is between –20 ~ 120°C. For cameras, even though they are used outdoors, they are typically held in the user’s hands. Thus, the temperature is always maintained around 0 ~ 40°C. Much above this temperature, the film will be damaged before the camera’s failure. On the other hand, requirements for automobile applications cover a much broader range: –50 ~ 150°C.

*Durability* – The standard requirement for the lifetime of office equipment such as printers is continuous operation for more than 3 months or 10<sup>11</sup> cycles. For cameras, it is only 5 × 10<sup>4</sup> cycles. Imagine how many pictures you take in a year. A 36-exposure roll of film may take months to use! Automobile applications usually require durability of more than 10 years. Other specs may include various tests such as mechanical shock/drop, humidity, air pressure (applications in air plane and in space).

In conclusion, the sequence for starting development will be:

*Camera > Office Equipment > Automobile.*

As we expected, piezo-actuators were first widely commercialized in a camera automatic focusing mechanism by Canon and in a shutter by Minolta. Then, they were employed in dot-matrix (NEC) and inkjet (Seiko EPSON) printers. Since piezo-multilayer actuators have been used in diesel injection valves (automobile) by Siemens in the 2000s, we



can say “the piezoelectric actuator development is in a maturing period.” It is notable that specs for cameras dramatically changed after shifting from film to digital. Digital cameras do not use film or mechanical shutters, leading to much more severe specs. The standard durability is NOT  $5 \times 10^4$  cycles anymore, because users started to take 10 times more pictures. The cyclic lifetime specs automatically increased by a factor of ten with digital cameras.

### 2.10.3 Consider the cost performance

We occasionally use a scoring sheet to identify a development target. How to score for narrowing down the development devices is demonstrated in **Figure 21**<sup>[23]</sup>. This table includes various factors which are essential, including financial factors (market and cost) and device performance. We compare the total scores, and select the higher priority for development (“pecking order”). The motor performance of the PZT-tube is better than that of the Metal-tube, while the Metal-tube endure the shock test. As initially claimed, the Metal-tube type is much cheaper in raw materials and manufacturing cost, because of the cheapest rectangular plate PZT usage. Regarding the marketing, the clients do not understand the inside “black box”; that is, PZT-tube or Metal-tube does not matter, as long as the device specs are satisfied.

**Figures 22(a), (b)** show the world-first camera module for Samsung flip cell phones commercialized in 2003. Newscale Technologies (Victor, NY) integrated a screw in the metal tube motor, and commercialized “squiggle motors” worldwide for camera module applications, with a partnership with ALPS, Tamron, and TDK-EPC<sup>[24]</sup>. Using PZT multilayer plates, replacing the original rectangular plates, the squiggle motors can be driven under 3 V, easy to be installed in compact portable equipment. Samsung Electromechanics is now utilizing much smaller micro ML chip linear USM’s for the Galaxy series camera modules due to the thinner design necessity<sup>[25]</sup>. **Figures 22(c), (d)** show the current camera module for Samsung Galaxy 6S smart phones in 2016. During 13 years, the camera module size was drastically reduced by 1/20.

**Reminder:** The development “pecking order” (i.e., the sequence for starting development) should be considered based on your company’s technology/capability (*Technological Creativity*). Then, using a *scoring table* in terms of “performance”, “cost” (*Product Planning Creativity*) and “market” (*Marketing Creativity*), the development focus can be narrowed down.

	Device A PZT tube	Device B Metal tube
<b>High Performance</b>		
1) figure of merit	0 1 ②	0 ① 2
2) Lifetime (shock test)	0 ① 2	0 1 ②
<b>Cheap Cost</b>		
3) raw materials cost	① 1 2	0 1 ②
4) preparation cost (machining, electroding)	① 1 2	0 1 ②
5) labor cost (special skill)	0 ① 2	① 1 2
<b>Good Market</b>		
6) design	0 1 ②	0 1 ②
7) production quantity	0 1 ②	0 1 ②
8) maintenance service	0 1 ②	0 1 ②
<b>Total score</b>	<b>10</b>	<b>13</b>

**Figure 21.** Scoring table for PZT-tube and Metal-tube motors for mobile phone applications.



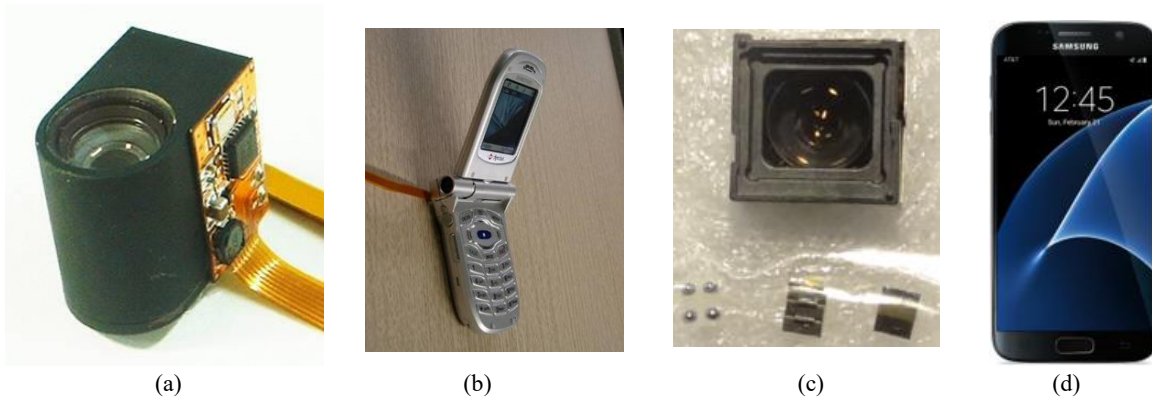


**Figure 22.** (a), (b) World first camera module for Samsung flip cell phones (2003), and (c), (d) current camera module for Samsung Galaxy 6S smart phones (2016).

### 3. Concluding remarks

My Ph.D. advisor was Late Prof. Shoiichiro Nomura at Tokyo Institute of Technology. When I joined his laboratory, he taught me first “Don’t read papers”. What is the real meaning of this? I had so-called “high academic grades” during my undergraduate period. I read many textbooks and academic journals. Accordingly, whenever Prof. Nomura suggested that I study a new research topic, I said things such as “that research was done already by Dr. XYZ, and the result was not promising ...” After having a dozen of these sort of negative conversations, partially angrily, partially disappointedly, Prof. Nomura ordered “Hey, Kenji! You are not allowed to read academic papers for a half year. You should concentrate on the following experiment without having any biased knowledge. Having a strong bias, you cannot discover new things. After finishing the experiment and summarizing your results, you are allowed to approach the published papers in order to find whether your result is reasonable, or is explainable by some theory.” Initially, I was really fearful of getting totally wrong results. However, I finished it. That led to my first discovery: PMN-PT electrostrictive materials.

Now I feel a similar dilemma to Late Prof. Nomura with my research associates, who are always seeking “Google” for finding out the research papers published. They start their research with this biased knowledge in order to fit the experimental results to the previous studies. Remember that knowing too much suppresses innovative work. A real discovery is usually made by a young less-experienced engineer. Once he/she becomes an expert professor, unfortunately he/she loses a sort of “creativity”. The “creativity” seems to be decayed with increasing the “knowledges” (except for the fundamental concepts).

The author hopes that the reader’s fundamental understanding on piezoelectric actuators became solidified, and that you can now discuss with your bosses, colleagues and associates on the development with much stronger confidence. I wish you to invent your breakthrough and innovative piezoelectric devices with the clear basic knowledge, without just chasing other researchers’ developments. I would not like to hear my associates’ excuse “I did it, because the previous researcher did so!”

### Acknowledgements

The author would like to acknowledge my former associates, who collected these misconceptions from the journal papers. Without those input, this article has not been realized. I am also appreciative of the research fund support from the US Office of Naval Research to ICAT/Penn State University (N00014-17-1-2088).

## References

---

1. Uchino K. *Ferroelectric Devices & Piezoelectric Actuators*, Lancaster, PA: DEStech Pub. Inc., 2017.
2. Uchino K. *Ferroelectric Devices 2nd Edition*, Boca Raton, FL: CRC Press, 2010.
3. Uchino K. *Micromechatronics 2nd Edition*, Boca Raton, FL: CRC Press, 2019.
4. Uchino K. Introduction to piezoelectric actuators: research misconceptions and rectifications. *Japan. J. Appl. Phys.* 2019; 58, <https://doi.org/10.7567/1347-4065/ab1645>
5. Du XH, Belegundu U, Uchino K. “Crystal Orientation Dependence of Piezoelectric Properties in Lead Zirconate Titanate: Theoretical Expectation for Thin Films,” *Japan. J. Appl. Phys.* 1997; Vol. 36 (9A): 5580-5587.
6. Wasa K. Proc. 69th ICAT Int’l Smart Actuator Symp., State College, PA, Oct. 4–5, 2016.
7. Muralt P. “Piezoelectric Thin Films For Mems”, *Integrated Ferroelectrics*. 1997; Vol. 17: 297–307.
8. Fujii F. Proc. Smart Actuators/Sensors Study Committee, JTTAS, Dec. 2, Tokyo, 2005.
9. Sugiyama S, Uchino K. “Pulse Driving Method of Piezoelectric Actuators”, Proc. 6th IEEE Int’l Symp. Appl. of Ferroelectrics, 1986, 637.
10. Uchino K. “Piezoelectric Actuators and Ultrasonic Motors”, Kluwer Academic Publishers, Norwell, PM, 1997, ISBN 0-7923-9811-4
11. Uchino K, Ishii T. “Mechanical Damper Using Piezoelectric Ceramics”, *J. Japan. Ceram. Soc.* 1988; 96(8): 863-867.
12. Muensit N. “Energy Harvesting with Piezoelectric and Pyroelectric Materials”, *Materials Science Foundations Vol. 72*, Trans Tech Pub., Stafa-Zuerich, Switzerland, 2011.
13. Uchino K, Ishii T. “Energy Flow Analysis in Piezoelectric Energy Harvesting Systems”, *Ferroelectrics*. 2010; 400: 305-320.
14. Kim HW, Priya S, Uchino K, Newnham RE. “Piezoelectric Energy Harvesting under High Pre-stressed Cyclic Vibrations” *J. Electroceramics*. 2005; 15: 27-34.
15. Kim HW, Priya S, Uchino K. “Modeling of Piezoelectric Energy Harvesting Using Cymbal Transducers” *Japan. J. Appl. Phys.* 2006; 45(7): 5836-5840.
16. Shekhani H, Scholehwar T, Hennig E, Uchino K. “Characterization of piezoelectric ceramics using the burst/transient method with resonance and antiresonance analysis,” *J. Am. Ceram. Soc.*; 2017; 100: 998.
17. Ural SO, Tuncdemir S, Zhuang Y, Uchino K. “Development of a high power piezoelectric characterization system (HiPoCS) and its application for resonance/antiresonance mode characterization”, *Japan. J. Appl. Phys.* 2009; 48: 056509.
18. Zhuang Y, Ural SO, Tuncdemir S, Amin A, Uchino K. “Analysis on Loss Anisotropy of Piezoelectrics with  $\infty$  mm Crystal Symmetry”, *Japan. J. Appl. Phys.*; 2010; 49, 021503.
19. Uchino K, Zhuang Y, Ural SO. “Loss Determination Methodology for a Piezoelectric Ceramic: New Phenomenological Theory and Experimental Proposals”, *J. Adv. Dielectrics*; 2011; 1, No. 1: 17-31.
20. Dong S, Lim SP, Lee KH, *et al.* “Piezoelectric Ultrasonic Micromotors with 1.5 mm Diameter”, *IEEE UFFC Trans* 2003; 50(4): 361-367.
21. Koc B, Cagatay S, Uchino K. “A Piezoelectric Motor Using Two Orthogonal Bending Modes of a Hollow Cylinder,” *IEEE Ultrasonic, Ferroelectric, Frequency Control Trans.* 2002; 49(4): 495-500.
22. Cagatay S, Koc B, Uchino K. “A 1.6 mm Metal Tube Ultrasonic Motor”, *IEEE Trans.- UFFC* 2003; 50(7): 782-786.
23. Uchino K. “Entrepreneurship for Engineers”, CRC Press, NY, 2009.
24. <https://www.newscatech.com/about-us/>
25. Koc B, Ryu J, Lee D, *et al.* 2006. Proc. New Actuator 2006 (Bremen, June 14-16), p. 58.